JAERI-M
90-071

DEVELOPMENT OF THYDE-HTGR: COMPUTER CODE FOR TRANSIENT THERMAL-HYDRAULICS OF HIGH-TEMPERATURE GAS-COOLED REACTOR

April 1990

Masashi HIRANO and Kazuhiko HADA

日本原子力研究所
Japan Atomic Energy Research Institute

JAERI-Mレポートは，日本原子力研究所が不定期に公刊している研究報告書です。
入手の問合わせは，日本原子力研究所技術情報部情報資料課（〒319-11茨城県那珂郡東海村）あて，お申しこしください。なお，このほかに財団法人原子力弘済会資料センター（〒319-11 茨城県那珂郡東海村日本原子力研究所内）で複写による実費頒布をおこなっております。

JAERI-M reports are issued irregularly.
Inquiries about availability of the reports should be addressed to Information Division Department of Technical Information, Japan Atomic Energy Research Institute, Tokai-mura, Naka-gun, Ibaraki-ken 319-11, Japan.

編集兼発行　日本原子力研究所
印　　刷　いばらき印刷㈱

JAERI-M 90-071

Development of THYDE-HTGR: Computer Code for Transient Thermal-Hydraulics of High-Temperature Gas-Cooled Reactor

Masashi HIRANO and Kazuhiko HADA

Department of HTTR Project
Oarai Research Establishment
Japan Atomic Energy Research Institute
Oarai-machi, Higashiibaraki-gun, Ibaraki-ken

(Received March 13, 1990)

The THYDE-HTGR code has been developed for transient thermal-hydraulic analyses of high-temperature gas-cooled reactors, based on the THYDE-W code. THYDE-W is a code developed at JAERI for the simulation of Light Water Reactor plant dynamics during various types of transients including loss-of-coolant accidents. THYDE-HTGR solves the conservation equations of mass, momentum and energy for compressible gas, or single-phase or two-phase flow. The major code modification from THYDE-W is to treat helium loops as well as water loops. In parallel to this, modification has been made for the neutron kinetics to be applicable to helium-cooled graphite-moderated reactors, for the heat transfer models to be applicable to various types of heat exchangers, and so forth. In order to assess the validity of the modifications, analyses of some of the experiments conducted at the High Temperature Test Loop of ERANS have been performed. In this report, the models applied in THYDE-HTGR are described focusing on the present modifications and the results from the assessment calculations are presented.

Keywords: Transient Thermal-hydraulic Analyses, High-Temperature Gas-Cooled Reactor, THYDE-HTGR Code, THYDE-W Code, Plant Dynamics

JAERI－M 90－071

高温ガス炉用過渡熱流力解析コード THYDE－HTGRの開発

日本原子力研究所大洗研究所高温工学試験研究炉開発部
平野　雅司・羽田　一彦

（1990年3月13日受理）

軽水炉のプラント動特性解析コードTHYDE－Wを改造して，高温ガス炉用過渡熱流力解析コードTHYDE－HTGRを開発した。THYDE－HTGRは，圧縮性気体または単相流，二相流に対する質量，運動量及びエネルギー方程式を解いて，それらの状態量の過渡変化を追跡する。THYDE－Wに対する主な修正は，水のループのみならずヘリウムのループも同時に取扱える機能を追加したこと，さらには，核動特性解析モデルをヘリウム冷却黒鉛減速の原子炉にも適用できるようにしたこと，高温ガス炉で用いる種々の熱交換器に適用できる熱伝達係数の相関式パッケージを追加したこと等である。本報告書では，こうした修正点を中心にTHYDE－HTGRの解析モデルを記述すると共に検証計算の結果を報告する。

大洗研究所：〒311－13　茨城県東茨城郡大洗町成田町字新堀3607

Contents

目　　次

Nomenclature

A : Flow area
A^H : Heat transfer area
B : Defined in Eq. (4.1.1-7)
C_i : Normalized concentration of i-th delayed neutron group
c_p : Specific heat
D : Hydraulic diameter
$\vec{F}$: Function vector
f : Fanning friction factor
f_{kn}, k=1,5 : Equations at node n
f^+_{kj}, k=1,2 : Equations at junction j
G : Mass flux
$\overline{G}$: Averaged mass flux
g : Gravitational acceleration
h : Specific enthalpy
$\overline{h}$: Averaged specific enthalpy
$\tilde{h}$: Specific enthalpy convected
h_{gl} : Latent heat
h_{tc} : Heat transfer coefficient
I : Defined in Eq. (4.1.1-7)
k : Thermal conductivity
L : Flow length
L_h : Elevation difference in node
L_{head} : External head
l : Neuton life
Nu : Nusselt number
n : Normalized neutron density
P : Pressure
$\overline{P}$: Averaged pressure
P^+ : Junction pressure
Pu : Prandtl number
q : Heat addition per unit volume
Re : Reynolds number
R_{ACT} : Normalized accinide power decay
R_{FP} : Normalized power decay from fission products
r : Coordinate
T : Temperature
t : Time
u : Velocity of phase k
V : Volume
$\vec{X}$: Variable vector
x : Quality
z : Coordinate

Greek letters

α : Void fraction
β : Delayed neutron fraction
β_i : Delayed neutron fraction of i-th group
Δt : Time step width
ε : Emissivity or multiplier
φ : Two-phase multiplier
Γ_{tot} : Total reactivity
κ : Form loss coefficient
λ : Decay constant

μ : Viscosity
ρ : Density
σ : Stefan-Boltzmann constant
$\Delta\vec{X}$: Increment in variable vector

Subscripts/Superscripts

A : Inlet of node
c : Thermal conductor
E : Outlet of node
$from$: Upstream side
g : Gas
j : Junction Number
l : Liquid
k : Phase index
n : Node number or current time level
old : Old time level
r : Relative
s : Saturated state
to : Downstream side

1. Introduction

For the safety evaluation of the High-Temperature Engineering Test Reactor (HTTR)[1] developed at Japan Atomic Energy Research Institute (JAERI), the THYDE-HTGR code has been developed at JAERI. THYDE-HTGR is capable of transient thermal-hydraulic analyses not only for the HTTR but for general high-temperature gas-cooled reactors (HTGRs).

The HTTR is being designed to be a helium-gas-cooled and graphite-moderated reactor of 30 MW thermal power. Figure 1-1 schematically illustrates the HTTR cooling system and Fig. 1-2 shows the bird's eye view of the HTTR reactor vessel. The generated thermal power is transferred from the primary helium loop to two parallelly-operated secondary loops. One is the helium-gas loop, connected by a helium/helium intermediate heat exchanger (IHX) of 10 MW. Another is the pressurized water loop, connected by the primary pressurized water cooler (PWC) of 20 MW. The secondary helium loop and the pressurized water loop is connected by the secondary PWC of 10 MW. Figures 1-3 and 1-4 show the bird's eye views of the IHX and primary PWC, respectively. In order to simulate the plant dynamic behavior during miscellaneous transients, therefore, it is necessary to treat both helium and water loops connected by various types of heat exchangers. Moreover, the transient behaviors of two-phase steam/water flow should be simulated in addition to the single-phase water and helium flows, because it is considered that loss-of-coolant accidents (LOCAs) at the pressurized water loop is one of the most important design basis events (DBEs) for the evaluation of the structural integrity of heat transfer tubes in PWCs.

In the early stage of HTTR development, the VESPER[3] code was applied to its plant dynamics simulation. This code, however, had some problems. For example, it can treat both helium and single-phase water flows but not two-phase steam/water flow. In addition, since the helium is assumed to be incompressible to solve the conservation equations, the applicability might be questionable to the cases where the pressure transient plays an important role.

From these points of view, the development of THYDE-HTGR was started based on the THYDE-W code which has been developed at JAERI for transient thermal-hydraulic analyses of both single and two-phase flows during

miscellaneous transients including LOCAs at light water reactors (LWRs). The major modifications from THYDE-W are to treat helium flows as well as water flows.

The THYDE-P[4], -P1[5] and -P2[6] are the ancestor codes of THYDE-W. THYDE-P, P1 and P2 were developed for the evaluation of the emergency core cooling systems (ECCSs) during LOCAs of pressurized water reactors (PWRs). Accompanied by shift in the emphasis from LOCA to non-LOCA transients, several capabilities such as to simulate the plant control system and multiple loops coupled by heat exchangers or steam generators are added to THYDE-W. These series of THYDE codes have been assessed[7-18] through the large scale LOCA experiments such as LOFT[19]. As for an example of the application of these THYDE codes to the safety analyses of actual reactors, THYDE-P was modified and used for the safety evaluation of the reconstructed Japan Research Reactor-3[20].

Concerning the model for the transient two-phase flow analysis, the THYDE codes are considered to be in the same generation as the RELAP4 code[21]. Basically three conservation equations of mass, momentum and energy for two-phase mixture are solved with taking into account the velocity difference between two phases by the drift flux model[5,26]. On the other hand, in newer generation codes such as TRAC-PF1[21] and RELAP5/MOD2[22], a so-called two-fluid model is applied, where three conservation equations are solved for each phase.

As for the assessment of applicability of THYDE-HTGR to dynamics simulation analyses of a helium gas flow loop, the steady state and transient experiments have been analyzed of the intermediate heat exchanger (IHX) in the High Temperature Helium Test Loop[23] constructed and operated by Ishikawajima-Harima Heavy Industry Co., Ltd. (IHI) under the programme of ERANS have been analyzed. The models to be assessed are the heat exchanger models including both heat transfer and hydraulics. The calculated results are in good agreement with the experimental data, and therefore the applicability of THYDE-HTGR to the high temperature helium gas loop with IHX has been verified. In this report, the results from the assessment calculations are presented together with the description of THYDE-HTGR focusing on the present modifications.

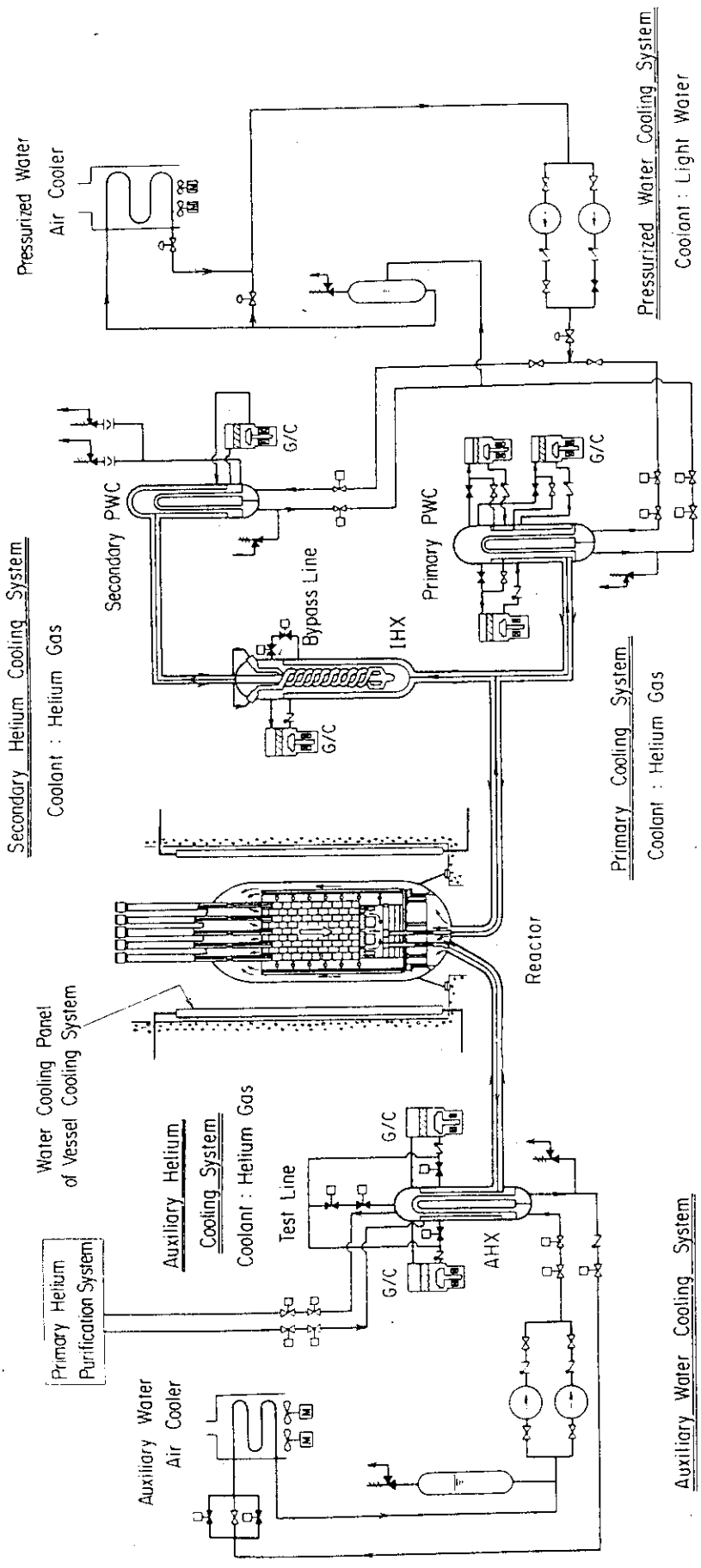

Fig. 1-1 Schematic Illustration of HTTR Cooling System

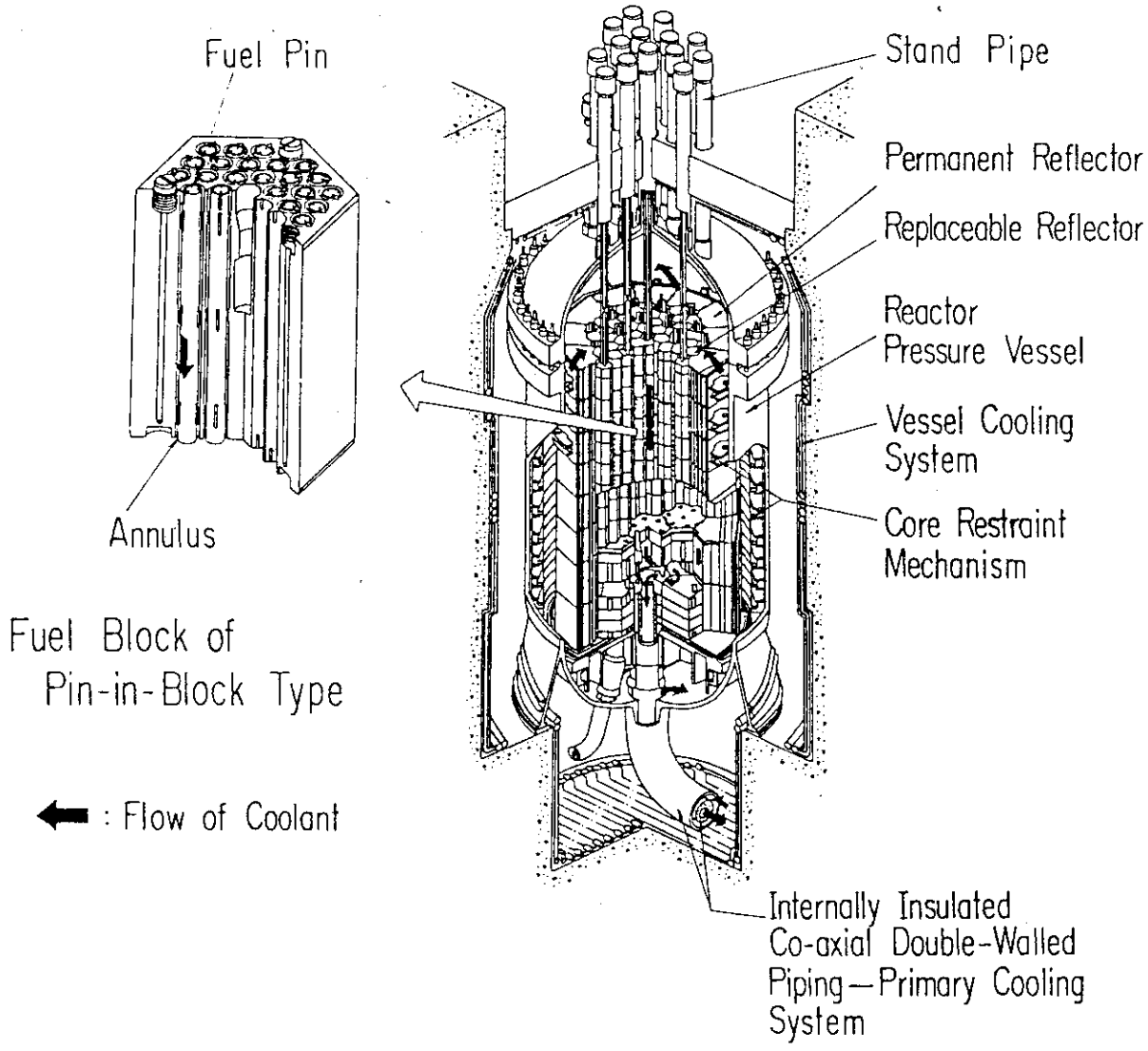

Fig. 1-2 Bird's Eye View of HTTR Reactor

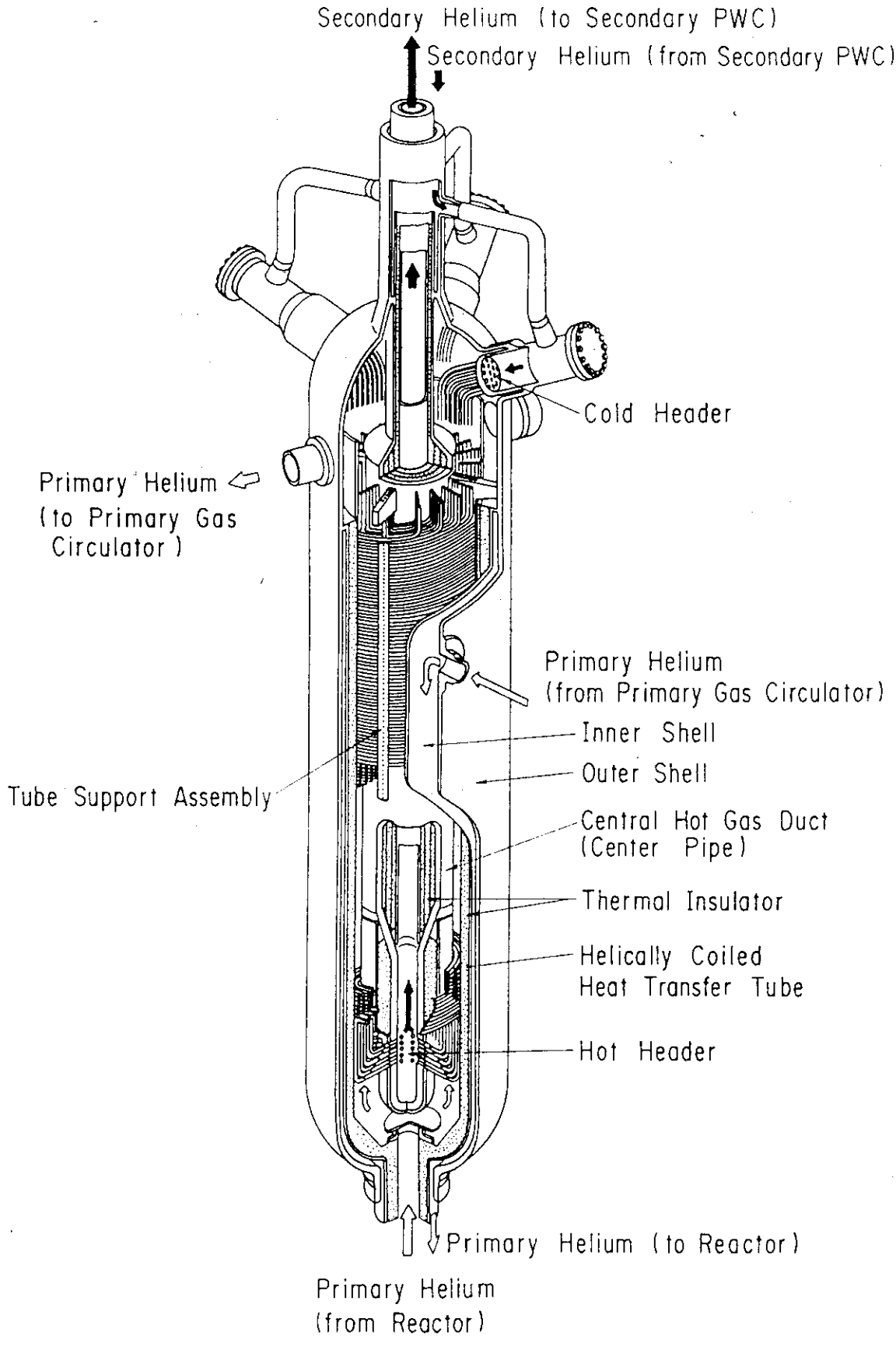

Fig. 1-3 Bird's Eye View of Intermediate Heat Exchanger of HTTR

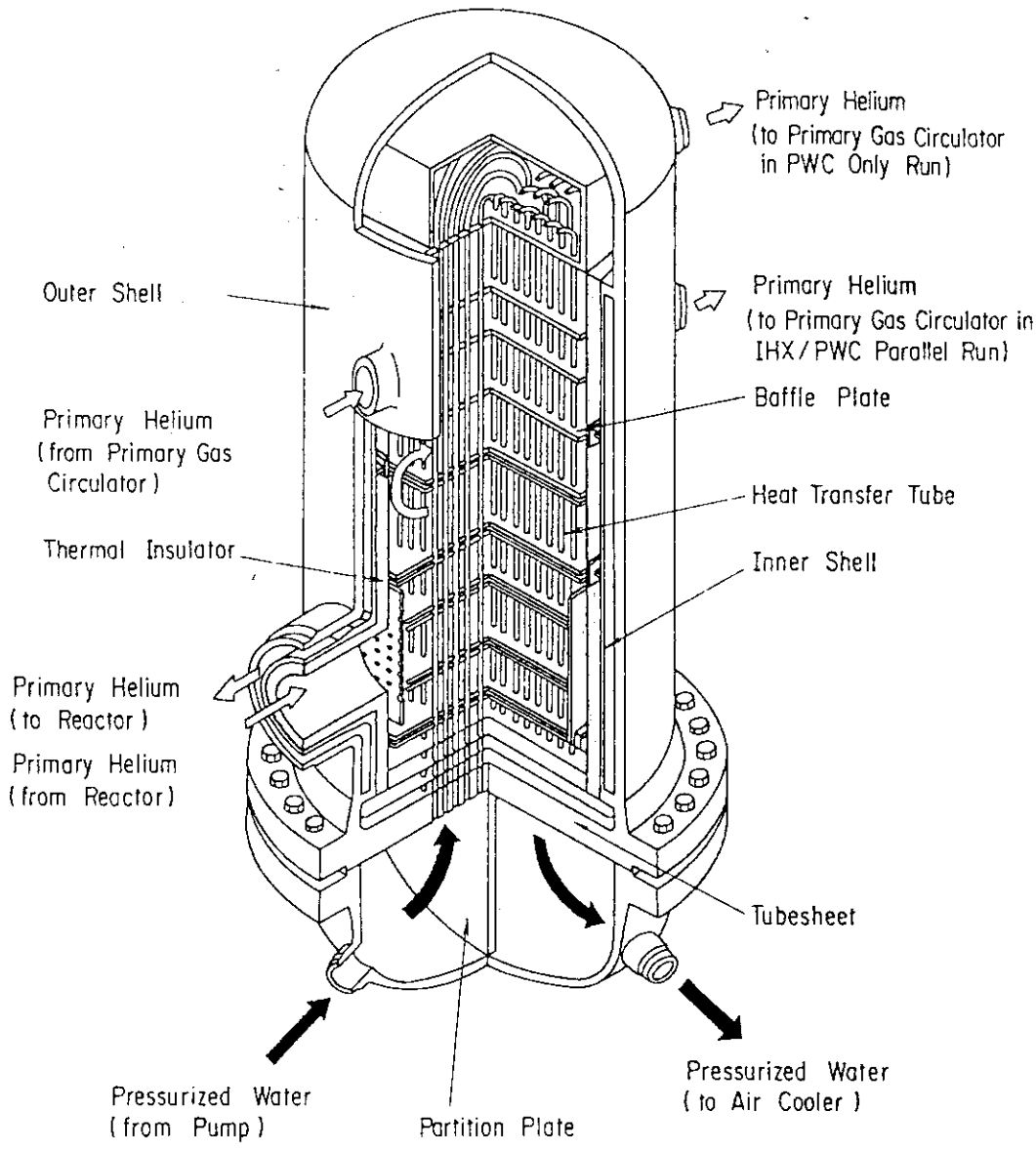

Fig. 1-4 Bird's Eye View of Primary Pressurized Water Cooler

2. Characteristics of Thermal-Hydraulic Analyses of HTGR

In this section, the characteristics of transient thermal-hydraulic analyses of HTGRs are discussed and then, at the same time, the reasons why the THYDE-W code was selected as a base code to be modified for HTGR analyses are clarified.

The characteristics of transient thermal-hydraulic analyses of HTGRs are summarized as follows from the view point of the safety evaluation differing from those of LWRs:

(1) The transient responses of the fuel rods to the miscellaneous disturbances induced at the primary and secondary loops are quite slow and mild, because the heat capacity of the graphite core structures such as moderators is much larger than that in LWR.

(2) On the contrary to (1), the transient responses of the coolant to the initiation events such as a termination of gas circulators, break at pipings, etc. are quite fast, because the flow inertia and heat capacity of a coolant gas are much smaller than those of water.

(3) The structural integrity is of special importance since the primary coolant temperature at reactor outlet is very high. Therefore, the gas should be treated compressible to evaluate the pressure transient, which is important as well as temperature transient for the evaluation of the integrity.

(4) Related to (3), transient two-phase flow analyses of water are involved for the evaluation of the structural integrity of the heat transfer tubes in PWCs. It is because a LOCA at the pressurized water loop has to be taken into consideration.

It was suggested from above characteristics that the numerical solution scheme of the conservation equations plays an important role. The reasons are the following. Although the early fast transients affect little the response of the core region, a short time step width is usually required to simulate such fast transients. In this case, the numerical

stability to allow large time step beyond the Coulant criteria[xx] is necessary because it is not always necessary to follow the fast transients. This can be realized by a fully implicit solution scheme. In the later part of the transient, on the other hand, it becomes a quasi-steady state and it requires a long time duration to be analyzed. In this case, also the fully implicit scheme is a powerful one. For the sake of safety evaluation of system thermal-hydraulics, although the gas should be treated compressilble, the pressure wave propagation, which is usually very fast in comparison with the flow velocity, is of no interest. In this case, again, the fully implicit scheme might be required to eliminate the pressure wave propagation and only to trace the gas flows. Corresponding to these considerations, the advantages to use the THYDE-W code as a base are summarized as follows:

(1) Two-phase steam/water flow can be treated.
(2) Fluids are treated compressible.
(3) A non-linear fully implicit scheme is applied to solve the conservation equations.

In addition to these, One of the advantages is that modifications are relatively easy, since the code has originally been developed at JAERI.

3. Characteristic Features of THYDE-HTGR

In this section, a brief description of the ancestor code THYDE-W and the major present modifications in THYDE-HTGR are summarized.

3.1 Brief Description of THYDE-W

THYDE-W has been developed based on THYDE-P2, the models and methods of which are described in detail in Ref. (5). The major capabilities added in THYDE-W are i) to simulate multiple loops coupled by heat transfers and ii) to simulate control systems. In addition to these miscellaneous modifications to enhance the capability to simulate non-LOCA transients have been performed. The major characteristic features of THYDE-W related to HTGR analyses are summarized as follows:

stability to allow large time step beyond the Coulant criteria[xx] is necessary because it is not always necessary to follow the fast transients. This can be realized by a fully implicit solution scheme. In the later part of the transient, on the other hand, it becomes a quasi-steady state and it requires a long time duration to be analyzed. In this case, also the fully implicit scheme is a powerful one. For the sake of safety evaluation of system thermal-hydraulics, although the gas should be treated compressilble, the pressure wave propagation, which is usually very fast in comparison with the flow velocity, is of no interest. In this case, again, the fully implicit scheme might be required to eliminate the pressure wave propagation and only to trace the gas flows. Corresponding to these considerations, the advantages to use the THYDE-W code as a base are summarized as follows:

(1) Two-phase steam/water flow can be treated.
(2) Fluids are treated compressible.
(3) A non-linear fully implicit scheme is applied to solve the conservation equations.

In addition to these, One of the advantages is that modifications are relatively easy, since the code has originally been developed at JAERI.

3. Characteristic Features of THYDE-HTGR

In this section, a brief description of the ancestor code THYDE-W and the major present modifications in THYDE-HTGR are summarized.

3.1 Brief Description of THYDE-W

THYDE-W has been developed based on THYDE-P2, the models and methods of which are described in detail in Ref. (5). The major capabilities added in THYDE-W are i) to simulate multiple loops coupled by heat transfers and ii) to simulate control systems. In addition to these miscellaneous modifications to enhance the capability to simulate non-LOCA transients have been performed. The major characteristic features of THYDE-W related to HTGR analyses are summarized as follows:

(1). The system to be analysed is discretized by the computational volumes called nodes and Junctions, which connect the nodes. The conservation equations of mass, momentum and energy for compressible singe- or two-phase flows are solved to these elements to determine the transient states of the dependent variables.

(2) Temperature distributions in the heat structural materials such as ducts, heat transfer tubes etc. are obtained by so-called heat slab module, which solves the one-dimensional transient heat conduction equation. The heat transfer rates to and/or from the fluids are evaluated using the heat transfer coefficients, evaluated by the own empirical correlation package, which considers both pre- and post-critical heat flux (CHF) heat transfer regimes.

(3) One point nuclear kinetic equations are solved to supply one of the heat sources to the heat slab, taking into account the reactivitis due to feedback effects and control rod insertion. The decay heats from fission products are also modeled.

(4) The components and equipments such as pumps, valves, injection systems are appropriately modeled.

(5) Loss-of-coolant through break are modeled considering the critical flow.

(6) The capability to setup the steady state prior to the transient calculation is incorporated.

(7) Automatic time step control is incorporated.

3.2 Summary of Modifications in THYDE-HTGR

The inevtable modification from THYDE-W to THYDE-HTGR is to treat helium as well as water because the primary coolant of HTGR is the helium

gas. The basic philosophy of the modification is that the numerics of the conservation equations should remain essentially unchanged and only the physical properties of water, which are given by so called steam table routines, are replaced by those of helium in case of helium flow. The modification have been performed without losing any capabilities of THYDE-W. The major code modifications done are summarized as follows:

(1) As for the state equation of the fluid, helium can be selected in addition to water,

(2) The heat transfer correlations applicable to describing the heat transfer behavior of helium flows in HTGRs have been selected and implemented as a correlation package,

(3) The numerical solution scheme has been modified, taking into account the difference in the heat capacity between water and helium,

(5) Radiation heat transfer between structures has been taken into consideration, since the structures of HTGRs are in service at high temperatures,

(6) Feedback reactivity due to change in temperature of moderator in graphite core has been treated,

(7) The physical properties of the heat conductor materials commonly used for HTGR have been implemented.

As for (1), since generally in transient thermal-hydraulic analysis codes, the physical property tables of fluids are refferred in many subroutines with different situations, the amount of the code modification related to this has been enormous. The physical properties of helium and structual materials implemented in the present work stated in (1) and (7) are described in detail in App. A. The modifications related to (2) to (6) will be described in the next section.

4. Models and Methods in THYDE-HTGR

In this section, the major models and methods applied in THYDE-HTGR are described. As already mentioned, THYDE-HTGR has been developed based on THYDE-W, the major models of which are described in Secs. 4.1 to 4.3. More detailed description is shown in Ref. (5). The major modification to THYDE-HTGR is described in Sec. 4.4.

4.1 Thermal-Hydraulic Models

4.1.1 Basic Field Equations

The basic field equations concerned are one-dimensional conservation equations of mass, momentum and energy for two-phase mixture shown as follows[5]:

$$A\frac{\partial}{\partial t}\rho + \frac{\partial}{\partial z}AG = 0 \ , \tag{4.1.1-1}$$

$$A\frac{\partial}{\partial t}G + \frac{\partial}{\partial z}\{(\alpha\rho_g u_g^2+(1-\alpha)\rho_l u_l^2)A\}$$

$$= - A\frac{\partial}{\partial z}P - \frac{A}{2}(\frac{\kappa}{L}+\frac{F}{D_h}\Phi_{tp})\frac{G|G|}{\rho} + A\rho g \ , \tag{4.1.1-2}$$

$$A\frac{\partial}{\partial t}\rho h + \frac{\partial}{\partial z}\{(\alpha\rho_g u_g h_g+(1-\alpha)\rho_l u_l h_l)A\} = Aq \ , \tag{4.1.1-3}$$

where

$$\begin{aligned} \rho &= \alpha\rho_g + (1-\alpha)\rho_l \ , \\ G &= \alpha\rho_g u_g + (1-\alpha)\rho_l u_l \quad \text{, and} \\ h &= xh_g + (1-x)h_l \ . \end{aligned} \tag{4.1.1-4}$$

A : Flow area
D_h : Hydraulic diameter
F : Fanning friction factor
G : Mass flux
g : Gravitational acceleration

h : Specific enthalpy of two-phase mixture
h_k : Specific enthalpy of phase k
L : Flow length
P : Pressure
q : Heat addition per unit volume
t : Time
u_k : Velocity of phase k
x : Quality ($=\alpha\rho_g/\rho$)
z : coordinate
α : Void fraction
Φ_{tp} : Two-phase multiplier
κ : Form loss coefficient
ρ : Mixture density
ρ_k : Density of phase k

Subscripts

g : Gas phase
l : Liquid phase

It should be noted that the kinetic energy terms are neglected in Eq.(4.1.1-3). The field equations for single-phase liquid, and single-phase steam and helium are corresponding to these equations with $\alpha = 0$ and $\alpha = 1$, respectively. The momentum and energy equations of Eqs.(4.1.1-2) and (4.1.1-3) can be rewritten in terms of the relative velocity u_r as follows:

$$A\frac{\partial}{\partial t}G + \frac{\partial}{\partial z}\{(\frac{G^2}{\rho}+B)A\}$$

$$= -A\frac{\partial}{\partial z}P - \frac{A}{2}(\frac{\kappa}{L}+\frac{F}{D_h}\Phi_{tp})\frac{G|G|}{\rho} + A\rho g \ , \qquad (4.1.1\text{-}5)$$

$$A\frac{\partial}{\partial t}\rho h + \frac{\partial}{\partial z}\{(hG - I)A\} = Aq \ , \qquad (4.1.1\text{-}6)$$

where

$$B = \frac{\alpha(1-\alpha)\rho_g\rho_l}{\rho}u_r^2 \ ,$$

$$I = \frac{\alpha(1-\alpha)\rho_g\rho_l h_{gl}}{\rho^2} u_r \quad . \tag{4.1.1-7}$$

h_{gl} : Latent heat

u_r : Relative velocity ($=u_g-u_l$)

When the relative velocity u_r in the above equations is assumed to be zero, the model is called a homogeneous model. In THYDE codes, the relative velocity is evaluated using the drift flux model[5,26].

The basic dependent variables to solve Eqs. (4.1.1-1), (4.1.1-5) and (4.1.1-6) are taken as P, h and G. The state equation gives the density ρ as a function of pressure and enthalpy as

$$\rho = \rho(P, h) \quad , \tag{4.1.1-8}$$

which is given by material property tables, depending on either water or helium in THYDE-HTGR. In the case of two-phase water flow, the density is obtained by the following way. When assumed the thermal equilibrium between two phases, the following expression can be obtained:

$$\rho = \alpha\rho_{gs}(P)+(1-\alpha)\rho_{ls}(P) \quad ,$$

$$\alpha = x\rho / \rho_{gs}(P) \quad ,$$

and

$$x = \{h-h_{gs}(P)\} / h_{gl}(P) \quad . \tag{4.1.1-9}$$

ρ_{ks} : Saturated density of phase k

h_{ks} : Saturated enthalpy of phase k

In THYDE codes, a model[6,16,17] to take into account the thermal non-equilibrium effects is implemented as well as the equilibrium model. The model has been developed and used in conjunction with condensation followed by cold ECC water injection during LOCAa at LWRs.

4.1.2 Node and Junction Equations

The conservation equations (4.1.1-1), (4.1.1-5) and (4.1.1-6) are

integrated, or in other words, differenced in a finite volume element called nodes, which are linked by junctions. There are several kinds of nodes and junctions as described in Ref. (5). In this section, for simplicity, only basic components called a normal node, a nomal junction and a mixing junction are described. The normal junction has no volume and connects two nodes. The mixing junction, however, has a finite volume and connects more than two nodes. The basic dependent variables assigned at the node n and and junction j are shown in Fig.4.1.2-1. The pressures P_n^A, P_n^E and mass fluxes G_n^A, G_n^E are assigned at the inlet (point A) and outlet (point E) of the node n. The node-averaged mass flux $\overline{G_n}$ and pressure $\overline{P_n}$ are assumed as follows:

$$\overline{G_n} = (G_n^A + G_n^E)/2 \ ,$$

and

$$\overline{P_n} = (P_n^A + P_n^E)/2 \ . \qquad (4.1.2\text{-}1)$$

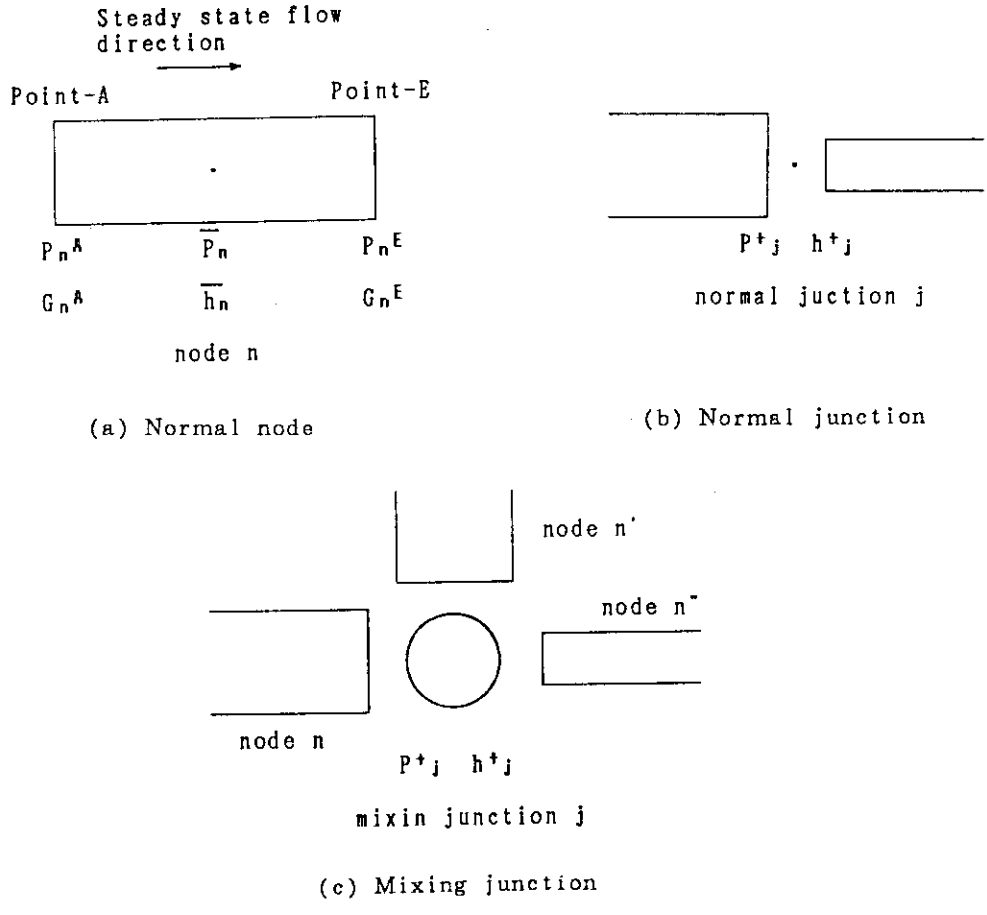

Fig. 4.1.2-1 Dependent Variables Assigned at Nodes and Junctions

The node-averaged specific enthalpy $\overline{h_n}$ is assigned at the node n. The enthalpies h_n^A and h_n^E at A and E points of the node n, respectively, are essentially the same as the the convective enthalpies $\tilde{h}_n^A$ and $\tilde{h}_n^E$, each of which means the averaged enthalpy at upstream nodes or upstream mixing junction. The node-averaged density $\overline{\rho}$ and densities ρ_n^A and ρ_n^E at points-A and -E of the node n are written as follows:

$$\overline{\rho_n} = \rho(\overline{P_n},\ \overline{h_n}) \ ,$$
$$\rho_n^A = \rho(P_n^A,\ h_n^A) \ ,$$

and

$$\rho_n^E = \rho(P_n^E,\ h_n^E) \ . \qquad (4.1.2\text{-}1)$$

At mixing junctions,

$$\rho_j^+ = \rho(P_j^+,\ h_j^+) \ ,$$

where the superscript + denotes the variables assigned at jucnctions. In terms of the variables described above, the basic field equations are discretized. As for the time integration in THYDE-W, almost all the terms are treated implicitly. Only the heat input to coolant q and external head L_{head} are treated explicitly. The conservation equations of mass, momentum and energy, Eqs. (4.1.1-1), (4.1.1-5) and (4.1.1-6), respectively, of the node n are discretised follows:

$$f_{1n} = -L_n\frac{\overline{\rho}_n - \overline{\rho}_n^{old}}{\Delta t} + G_n^A - G_n^E = 0 \ , \qquad (4.1.2\text{-}2)$$

$$f_{4n} = -L_n\frac{G_n^A + G_n^E - G_n^{A,old} - G_n^{E,old}}{2\Delta t} + P_n^A - P_n^E + \Phi_n^A - \Phi_n^E$$
$$-\frac{1}{2}\left(\frac{K_n}{L_n} + \frac{F_n}{D_{h,n}}\Phi_{tp,n}\right)\frac{\overline{G}_n|\overline{G}_n|}{\overline{\rho}_n} + \overline{\rho}_n g(L_h - L_{head}^{old})_n = 0 \ , \qquad (4.1.2\text{-}3)$$

$$f_{5n} = -L_n\frac{\overline{\rho}_n\overline{h}_n - \overline{\rho}_n^{old}\overline{h}_n^{old}}{\Delta t} + G_n^A\tilde{h}_n^A - G_n^E\tilde{h}_n^E + I_n^A - I_n^E +$$
$$+ q_nL_n = 0 \ , \qquad (4.1.2\text{-}4)$$

where

$$\Phi_n^A = \frac{G_n^{A2}}{\rho_n^A} + B_n^A \ ,$$

and

$$\Phi_n^E = \frac{G_n^{E2}}{\rho_n^E} + B_n^E \ .$$

L_h : Elevation from inlet to outlet.

The superscript *old* denotes the value at one time step before the current time. Further, in order to couple the pressures P_n^A and P_{from}^+ at the inlet of the node n and its ajacent junction, respectively, and those P_n^E and P_{to}^+ at the outlet of the node n and its ajacent junction, respectively, the following equations are solved:

$$f_{2n} = (\xi_n^A)^2(P_{from,n}^+ - P_n^A - \Phi_n^A/2) - (1-\xi_n^A)\ G_n^A \qquad (4.1.2\text{-}5)$$
$$- \frac{\kappa_n^A \Phi_{tp}}{2\rho_{fn}^A}\ G_n^A |G_n^A| = 0 \ ,$$

$$f_{3n} = (\xi_n^E)^2(-P_{to,n}^+ + P_n^E + \Phi_n^E/2) - (1-\xi_n^E)\ G_n^E \qquad (4.1.2\text{-}6)$$
$$- \frac{\kappa_n^E \Phi_{tp}}{2\rho_{fn}^E}\ G_n^E |G_n^E| = 0 \ .$$

where ξ is a parameter to express valve behaviors. Here we assume a valve is located inbetween two successive nodes n-1 and n. When the valve is completely opened, ξ is equal to one and therefore, Eqs. (4.1.2-5) and (4.1.2-6) lead to simply

$$P_{n-1}^E + \Phi_{n-1}^E/2 = P_n^A + \Phi_n^A/2 \ , \qquad (4.1.2\text{-}7)$$

because $P_{to,n-1}^+ = P_{from,n}^+$. On the other hand, when the valve is completely closed, ξ is set equal to zero and, in this case, the mass fluxes G_{n-1}^E and G_n^A are solved to be zero from Eq.(4.1.2-5) and (4.1.2-6).

The equations to be solved for a normal junction j are shown as follows:

$$f_{1j}^+ = A_{n,from} G_{n,from}^E - A_{n,to} G_{n,to}^A = 0 \ , \qquad (4.1.2\text{-}8)$$

$$f_{2j}^+ = h_j^+ - \tilde{h}_j = 0 \ , \qquad (4.1.2\text{-}9)$$

where $\tilde{h}_j$ is essentially the averaged enthalpy of the upstream side of the node or mixing junction. The equations for a mixing junction j are shown as follows:

$$f^+_{1j} = \Sigma_{in} A_n G^E_n - \Sigma_{out} A_n G^A_n - V_j(\overline{\rho}^+_j - \overline{\rho}^{+old}_j) / \Delta t = 0 \ , \qquad (4.1.2\text{-}10)$$

$$f^+_{2j} = \Sigma_{in} A_n G^E_n \tilde{h}^E_n - \Sigma_{out} A_n G^A_n \tilde{h}^A_n - V_j(\overline{\rho}^+_j h^+_j - \overline{\rho}^{+old}_j h^{+old}_j) / \Delta t \qquad (4.1.2\text{-}11)$$

$$= 0 \ .$$

4.1.3 Numerical Solution Procedure

The discretized equation system described in the preceding section is solved based on the well-known Newton-Raphson method. The increment $\Delta \vec{X}_m$ in the dependent variable vector $\vec{X}$ at the m-th iteration step is expressed by the inverse of the Jacobian matrix J and the system equation vector $\vec{F}$ as follows:

$$\Delta \vec{X}_m = -J^{-1}(\vec{X}_m) \ \vec{F}(\vec{X}_m) \ . \qquad (4.1.3\text{-}1)$$

The iteration procedure is repeated until a conversion criteria is satisfied[5], with updating the Jacobian matrix at each iteration step. The detailed procedure including the method for the Jacobian matrix inversion, Ref. (5) should be referred.

4.2 Heat Conductor Model

A generalised one-dimensional heat conductor model, which is called a heat slab model, is implemented to simulate the temperature transients within structural materials such as fuel rods, heat transfer tubes in heat exchangers, duct walls, etc. In this model, one-dimensional thermal conduction equation is solved either in cartesian or cylindrical coordinate, where several types of boundary conditions are prepared for both left-hand-side and right-hand-side boundaries. For the case, for example,

that the boundaries are in contact with fluids, each heat transfer coefficent is evaluated by the own correlation package depending on either the fluid is water or helium. The heat sources within the structural materials are either given by inputs as time tables or by solving the one-point nuclear kinetic equation considering the decay heat after shutdown. The physical properties of the structural materials are also given by inputs or by the built-in table data.

4.2.1 One-Dimensional Thermal Conduction Equation

The equation solved in the heat conductor model is the one-dimensional thermal conduction equation, shown as follows:

$$(\rho c_p)_c \frac{\partial T_c}{\partial t} = \frac{1}{r^a}\frac{\partial}{\partial r}(k_c r^a \frac{\partial T_c}{\partial r}) + \Xi \ . \qquad (4.2.1\text{-}1)$$

where

a = 0 for cartesian coordinate
= 1 for cylindrical coordinate

k_c : Thermal conductivity of conductor
r : Coordinate
T_c : Temperature of conductor
$(\rho c_p)_c$: Volumetric heat capacity of conductor
Ξ : Heat source per unit volume

The thermal conduction equation Eq.(4.2.1-1) is discretized in time and space and numerically solved. The detailed information on the numerical solution procedure is shown n Ref. (5). The heat conductor model is coupled with the energy conservation equation of node, shown in Eq. (4.1.2-4), through the heat input to coolant per unit volume of the node q in Eq. (4.1.2-4), which is evaluated by

$$q_n = \sum_k A_k^h \, h_{tc,k} \, (T_{w,k} - T_n) / V_n \ , \qquad (4.2.1\text{-}2)$$

A_k^h : Heat transfer area of slab k

$h_{tc,k}$: Heat transfer coefficient at surface of slab k

$T_{w,k}$: Surface wall temperature of slab k

T_n : Bulk temperature of node n

V_n : Volume of node n

where the summation is taken all the heat slabs faced to the node n. In general, the heat transfer coefficient is dependent on the variables in the node n and the node n side of the wall temperature of heat slab k. The heat transfer coefficient $h_{tc,k}$ is evaluated by one of the the empirical correlations in the correlation packages. In THYDE-HTGR, two kinds of the heat transfer correlation packages are incorporated, i.e. one is for both singe-phase and two-phase water flows and another is for helium flow. The former is summarized in Tables 4.2.1-1 to 4.2.1-3 and the latter, which is developed in the present work, will be described in Sec. 4.4.2.

Since the heat exchanger model plays an important role in HTGR dynamics analyses, the model is described hereafter as an example of the usage of the heat slab model. Figure 4.2.1-1 shows the typical nodalization of the heat exchanger, which consists of nodes and junctions to simulate primary side and secondary side flows, and the heat slabs to simulate one of the heat transfer tubes. This nodalization represents the average behavior of the total number of flow paths with one tube each. In THYDE codes, the bulk temperature T_n is defined as follows:

$$T_n = T(\bar{P}_n, \bar{h}_n) \quad . \tag{4.2.1-3}$$

It should be noted that when this definition is taken, the temperature difference between the primary and secondary fluids are underestimated especially for the counter flow type of heat exchangers as shown in Fig. 4.2.1-2, which schematically shows the comparison between the calculated temperature distribution and actual one for the nodalization shown in Fig. 4.2.1-1. The advantage to take this definition is the numerical stability especially to the cases with flow stagnation and flow reversal and this advantage is important in view of the system dynamics analyses.

Table 4.2.1-1 CHF Correlations for Water

Option	Condition	Correlation
1	$G>G_t$	Biasi[27]
2		GE[28]
3		Model in RELAP4[20]
1	$G<G_t$	Interpolation between CHF($G=G_t$) and $9\cdot10^4$ $Btu/ft^2\cdot hr$($G=0$)
2		Modified Zuber[29]
3		Zuber[29]

Table 4.2.1-2 Heat Transfer Corelations for Water

Mode	Conditions	Correlation
10	$T_b, T_w<T_s, Re>2000$	Dittus-Boelter[30]
11	$T_b, T_w<T_s, Re<2000$	See Ref.(5)
20/21	$T_b<T_s<T_w$	Interpolation between Modes 10 or 11 and 31
20/22	$T_b<T_s<T_w$	Interpolation between Modes 10 or 11 and 32
31	$T_b=T_s, T_s<T_w, \varphi<\varphi_{CHF}$	Jens-Lottes[31]
32	$T_b=T_s, T_s<T_w, \varphi<\varphi_{CHF}$	Thom[32]
41-45	$T_b=T_s, T_s<T_w, \varphi>\varphi_{CHF}$	See Table 4.2.1-3
50	$T_b=T_s, T_s>T_w$	Condensation[33]
51	$T_b>T_s, Re<3000$	Laminar steam flow cooling[34]
52	$T_b>T_s, 3000<Re<5000$	Interpolation between Modes 51 and 53
53	$T_b>T_s, 5000<Re$	McEligot[35]

Table 4.2.1-3 Post-CHF Correlations for Water

Mode	Conditions	Correlation
41	$x>0.5$, $G>G_t$ and $P>P_t$	Groenevelt[36]
42	$x>0.5$, $G>G_t$ and $P<P_t$	Dougall-Rohsenow[37]
43	$x<0.5$, $G>G_t$	Interpolation between Mode 41 or Mode 42($x=0.5$) and CHF($x=0$)
44	$G>G_t$	Berenson[38], Modified Bromley[39] or Bromley-Pomeranz[40]

G : Mass flux
G_t : Threshold mass flux (= 300 (kgm/cm^2 s))
P : Pressure
P_t : Threshold pressure (= 30 (kgf/cm^2))
Re : Reynolds number
T_b : Bulk temperature
T_s : Saturated temperature
T_w : Wall temperature
x : Quality
φ : Heat flux
φ_{CHF} : Critical heat flux

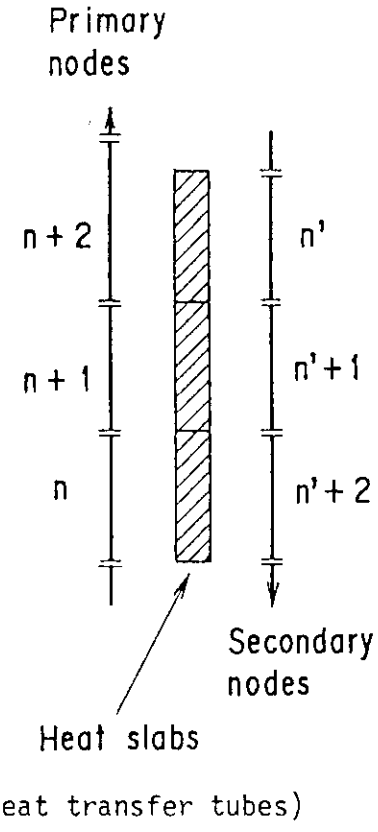

Fig. 4.2.1-1 Typical Nodalization Scheme for Heat Exchanger

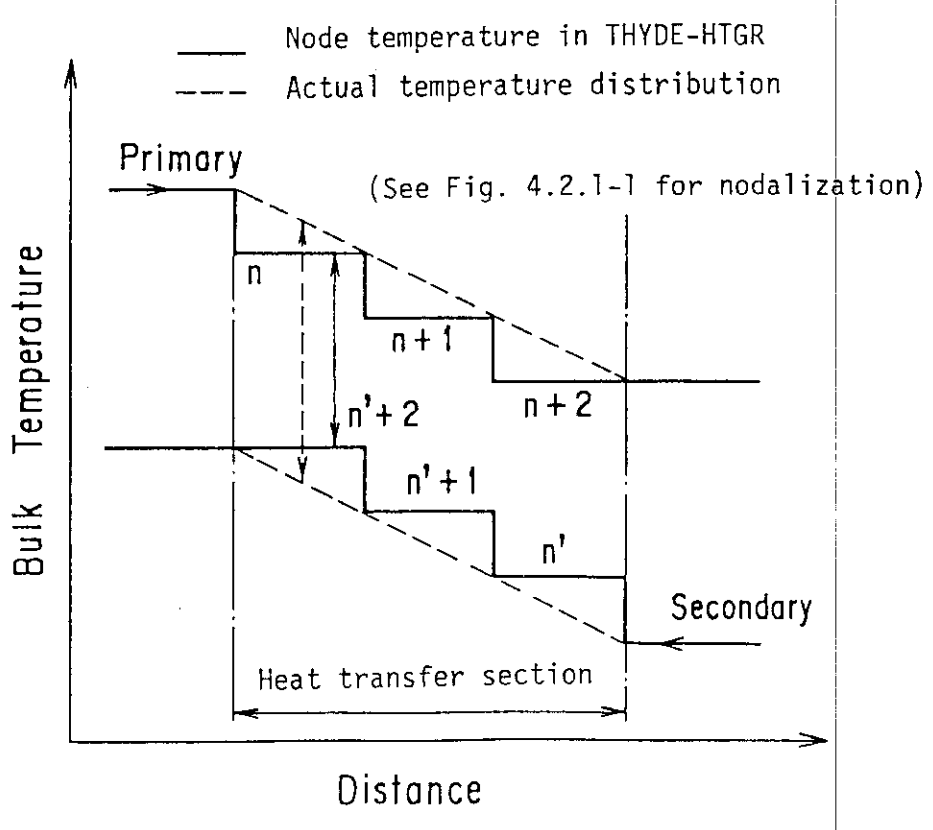

Fig. 4.2.1-2 Definition of Bulk Temperature

4.2.2 Heat Source in Fuel Rods

The fuel rods are simulated by the heat slab model described in the previous section. The model for the heat source in the fuel rods is, therefore, to provide one of the heat sources within the heat slab. As for the heat source, the fission power and decay heats from fission products are taken into consideration. The normalized total reactor power Π is shown as follows:

$$\Pi = \frac{n+\varepsilon R_{FP}+R_{ACT}}{1+\varepsilon R_{FP,0}+R_{ACT,0}} , \qquad (4.2.2\text{-}1)$$

Π : Normalized total reactor power
n : Normalized neutron density
R_{FP} : Normalized decay power from fission products
R_{ACT} : Normalized decay power of accinides
ε : Multiplier to decay power

where the subscript 0 denotes the steady state value and ε is an arbitrary multiplier specified by input and usually is taken to be 1.2 for safety evaluation purpose.

The normalized neutron density n is obtained by solving the one point nuclear kinetic equations:

$$\frac{dn}{dt} = \frac{\beta}{l}(\Gamma_{tot}-1)n + \sum_{i=1}^{6} \lambda_i C_i ,$$

$$\frac{dC_i}{dt} = -\lambda_i C_i + \frac{\beta_i}{l} n . \qquad (4.2.2\text{-}2)$$

where

$$\beta = \sum_{i=1}^{6} \beta_i ,$$

and

$$n_0 = 1$$

C_i : Concentration of delayed neutron group i

l : Neutron generation time

n : Reactor fission power

n_0 : Initial reactor fission power

β : Effective delayed neutron fraction

β_i : Effective fraction for delayed neutron group i

Γ_{tot} : Total reactivity

λ_i : Decay constant of delayed neutron group i

As for the total reactivity Γ_{tot}, i) reactiveity due to control rod insertion and ii) feedback reactivities are considered. The latter will be discussed later.

For the decay power from fission products except accinides, the model applied in the RELAP4 code[21] is used. In this model, the total decay heat is evaluated by 11 groups of decay heats with different decay constants as follows:

$$\frac{\gamma_j}{dt} + \lambda_j \gamma_j = E_j n, \quad (j=1,2,\ldots 11) \ , \tag{4.2.2-3}$$

γ_j : Concentration of decay heat group j

λ_j : Decay constant of decay heat group j

E_j : Yield fraction of decay heat group j

where the decay constants were obtained as shown in Table 4.2.2-1 by curve fitting to the equation by Shure[25] for step-wise reactor shutdown. For the power from accinide decay, the model in Ref. (25) is incorporated.

Table 4.2.2-1 Radioactive Decay Constants

Group	E_j	λ_j (s^{-1})
1	0.00299	1.772
2	0.00825	0.5774
3	0.01550	$6.743 \cdot 10^{-2}$
4	0.01935	$6.214 \cdot 10^{-3}$
5	0.01165	$4.739 \cdot 10^{-4}$
6	0.00645	$4.810 \cdot 10^{-5}$
7	0.00213	$5.344 \cdot 10^{-6}$
8	0.00164	$5.726 \cdot 10^{-7}$
9	0.00085	$1.036 \cdot 10^{-7}$
10	0.00043	$2.959 \cdot 10^{-8}$
11	0.00057	$7.585 \cdot 10^{-10}$

4.3 Summary of Component Models

The other major models related to HTGR analyses are briefly described in this section. These models are to supply constitutive relations to close the conservation equation system or boundary conditions to it.

(1) Pump Model

The pump model supplies L_{head} in Eq.(4.1.2-1) for both water pumps and helium circulators. The transient of the rotational speed is either given by inputs as time table or calculated by solving the equation of angular momentum of impeller-flywheel assembly. In order to obtain the head and torque, the homologous head and torque curves are given by inputs. In addition, the pump head and torque degradation due to two-phase flow is modeled.

(2) Valve Model

The dynamic behaviors of the valves are simulated by

$$\frac{d\xi}{dt} = \frac{\xi_c - \xi}{t} , \tag{4.3-1}$$

where

$\xi_c = 1$ when it is completely open

$= 0$ when it is completely closed .

The parameter ξ is corresponding to the valve opening ratio. In fact, as shown in Eqs.(4.1.2-5) and (4.1.2-6), the mass flux at the valve is calculated to be zero when $\xi=0$. And when $\xi=1$, these equations become identical to the momentum equations at junctions. The time constant t is an input and the logic to determine γ_c depends on the type of valves such as check valve, control valves.

(3) Break Flow Model

Critical flow models are implemented to evaluate the break flow at double-ended or split breaks. The models implemented for subcooled water

and saturated water are those proposed by Zaloudek[42] and Moody[43], respectively. The sonic chocking model[6] is used for superheated steam and helium.

(4) Trip and Control System Model

The action initiation and termination of component modeles such as control rod insersion, valves, breaks etc. are controlled by the trip model. The logic to trigger the trip signal can be composed by inputs. The plant control systems are simulated by the control system models. The control logic can be constructed by inputs from the basic control blocks implemented.

4.4 Modification in THYDE-HTGR

4.4.1 Implicit Scheme for Heat Addition to Node

The numerical solution procedure related to the heat addition to the coolant is modified in order to treat helium flow. In THYDE codes, the heat addition to coolant q in Eq. (4.2.1-2) is evaluated explicitly by using the variables one time step before the current time step shown as follows:

$$q_n = \sigma A_k^h h_{tc,k}^{old} (T_{w,k}^{old} - T_n^{old}) / V_n , \qquad (4.4.1-1)$$

and therefore, q_n is treated a constant in the Newton-Raphson iteration, which is stated in 4.1.3. In the present modification, the heat transfer rate q_n is treated partially implicitly. Namely, T_n^{old} in Eq. (4.4.1-1) is replaced by T_n, which is the value to be solved at the current time step. Before the modification, a numerical oscillation often occurred when the helium flow decreased to be nearly equal to zero. In this oscillation, the bulk temperature repeatedly goes above and below the wall temperature at every time step. This numerical phenomenon did not occur for water flow but occurs for helium flow because the heat capacity of helium gas is much smaller than that of water. This oscillation is avoided by the present modification and it enables us stable calculations with relatively large time step width.

4.4.2 Heat Transfer Correlation Package for Helium

The heat transfer correlation package has been developed and implemented in THYDE-HTGR for calculationg heat transfer rates in the HTGR core and two types of heat exchangers commonly used in HTGRs. As heat exchangers, the primary and secondary PWCs, as shown in Fig.1-3, and the Auxiliary Heat Exchanger (AHX) are the baffled shell-and-tube type, while the helium/helium IHX, shown in Fig.1-4, is the helically-coiled type. The correlations implemented in this package are for the following flows:

Category 1: reactor core flows

(1-1) Annulus channel simulating flow channels in a fuel block of pin-in block type
(1-2) Circular channels simulating flow channels in a fuel block of multi-hole type

Category 2: heat exchanger flows

(2-1) Inside and outside tubes of baffled shell-and-tube type of heat exchangers
(2-2) Inside and outside tubes of helically-coiled type of heat exchangers

These correlations are as follows:

(1-1) Annulus channel

The heat transfer rates from fuel pins of pin-in-block type to helium gas are evaluated by

$$Nu = \max(Nu_l, Nu_t) , \qquad (4.4.2\text{-}1)$$

where

$$Nu_l = c(\alpha)\ (T_b/T_w)^{0.5} \quad \text{for laminar flow,} \tag{4.4.2-2}$$

$$Nu_t = 0.020\alpha^{-0.16}\ Re^{0.8}\ Pr^{0.4}\ (T_b/T_w)^{0.5} \quad \text{for turbulent flow} \tag{4.4.2-3}$$

$$c(\alpha) = -4.8268\alpha^3 + 12.7516\alpha^2 - 12.2505\alpha + 9.7170\ . \tag{4.4.2-4}$$

c_p : Specific heat
d_i : Inner dia. of annulus, or outer dia. of fuel pin
d_o : Outer dia. of annulus, or inner dia. of coolant hole of fuel block
De : Equivalent diameter ($=d_o-d_i$)
k : Thermal conductivity of helium
Nu : Nusselt number ($=h_{tc}\cdot De/k$)
Pr : Prandtle number ($=c_p\cdot\mu/k$)
Re : Reynolds number ($=u_i\cdot De/\nu$)
T_b : Bulk temperature
T_w : Wall temperature
u_i : Average velocity of flow in channel channel
α : Diameter ratio d_i/d_o
μ : Viscosity
ν : Kinematic viscosity($=\mu/\rho$)

Equation (4.4.2-2) is given in Ref.(44). In Eq. (4.4.2-3), the constant is determined on the conservative side from experimental data by the HENDEL test facility[45], while the power numbers of α, Re, Pr and (T_b/T_w) are assumed from reviewing available information.

(1-2) Circular channel

$$Nu = \max(\ Nu_l,\ Nu_t\ )\ , \tag{4.4.2-5}$$

where

$$Nu_l = 4.36\ (T_b/T_w)^{0.5} \quad \text{for laminar flow, and} \tag{4.4.2-6}$$

$$Nu_t = 0.02\ Re^{08}\ Pr^{0.4}\ (T_b/T_w)^{0.5} \quad \text{for turbulent flow.} \tag{4.4.2-7}$$

Both equations are referred to GA's formula[46].

d_i : Diameter of circular flow channel

Nu : Nusselt number ($=h_{tc} \cdot d_i / k$)
Pr : Prandtle number ($=c_p \cdot \mu / k$)
Re : Reynolds number ($=u_i \cdot d_i / \nu$)
u_i : Average velocity of flow in channel

(2-1) Inside tube of baffled shell-and-tube type heat exchanger

$$Nu = \max(Nu_l, Nu_t), \tag{4.4.2-8}$$

where

$$Nu_l = 4 \quad \text{for laminar flow,} \tag{4.4.2-9}$$
$$Nu_t = 0.023\ Re^{0.8}\ Pr^{0.4} \quad \text{for turbulent flow.} \tag{4.4.2-10}$$

d_i : Inner diameter of tube
Nu : Nusselt number ($= h_{tc} \cdot d_i / k$)
Pr : Prandtle number ($=c_p \cdot \mu / k$)
Re : Reynolds number ($=u_i \cdot d_i / \nu$)
u_i : Average velocity of flow in channel

Equation (4.4.2-10) is the well-known Dittus and Boelter correlation[30].

(2-2) Outside tube flow of baffled shell-and-tube type heat exchanger

$$Nu_o = C_a \max(Re_o, Re_{min})^{0.6} Pr^{1/3} \mu^* , \tag{4.4.2-11}$$

where

C_a : constant, and
$$Re_{min} = 10.0 . \tag{4.4.2-12}$$

The minimum value of thr Reynolds number is taken from an advantage of the numerical analysis. The original form of Eq.(4.4.2-11) was proposed by D. A. Donohue[47], which is experimentally developed for baffled shell-and-tube types of heat exchangers.

The symbol μ^* denotes the ratio μ / μ_w of viscosity at bulk temperature

to that at wall temperature. The Reynolds number Re_o and Nusselt number Nu_o are defined, respectively, as follows:

$$Re_o = u_o d_o / \nu \quad , \text{ and} \tag{4.4.2-13}$$

$$Nu_o = \frac{h_{tc} \cdot d_o}{\kappa} \tag{4.4.2-14}$$

where

$u_o = Q / A_e$:weighted velocity,

$A_e = \sqrt{(A_c)_{Bh} \cdot (A_c)_{cross}}$:weighted flow area ,

$(A_c)_{Bh} = K_{Bh} \cdot \frac{\pi}{4} D_s^2$:Baffle-hole area ,

$(A_c)_{cross} = (D_s - Z_h d_0)\overline{BP}$:Cross-flow area .

$\overline{BP}$: Distance between baffle plates

d_o : Outer diameter of tube

D_s : Inside diameter of shell

K_{Bh} : Ratio of baffle-hole area to cross-sectional area of shell

Q : Volumetric flow rate

Z_h : Number of tubes at the centre of cross section of shell

(2-3) Inside tube flow of helically-coiled type heat exchanger

$$Nu = \max(Nu_l, Nu_t) , \tag{4.4.2-15}$$

where

$$Nu_l = 4.36\left(\frac{0.148\sqrt{Dean}}{1 - 1.813/\sqrt{Dean}}\right) \quad \text{for laminar flow, and} \tag{4.4.2-16}$$

$$Nu_t = 0.0223\, Re^{5/6}\, d_i^{*1/12} \frac{Pr}{(Pr^{0.6} - 0.057)} \left(1 + \frac{0.0615}{(Re\, d_i^{*2.5})^{1/6}}\right)$$

for turbulent flow. (4.4.2-17)

The non-dimensional number d_i^* is defined as d_i / Dm, where Dm is the

average diameter of helical coils. The Dean number *Dean* is defined as $Re\sqrt{d_i}$.

d_i : Inner diameter of tube
Nu : Nusselt number ($= h_{tc} \cdot d_i / k$)
Pr : Prandtle number ($= c_p \cdot \mu / k$)
Re : Reynolds number ($= u_i \cdot d_i / \nu$)
u_i : Average velocity of inner tube

Both Eqs.(4.4.2-16) and (4.4.2-17) were originally proposed by Mori and Watanabe[48], which are taken into account heat transfer enhancement by secondary flow in a curved tube. Numerical errors in deriving the original equation are corrected by one of the authors[49].

(2-4) Outside tube flow of helically-coiled type heat exchanger

$$Nu_o = 0.33\ C_h\ Re_o^{0.6}\ Pr^{0.3} \quad \text{for } Re_o \geqq 7000\ , \text{ and} \qquad (4.4.2\text{-}18)$$

$$Nu_o = \max(\ Nu_{ol},\ Nu_{ot}\ ) \quad \text{for } Re_o < 7000\ , \qquad (4.4.2\text{-}19)$$

where

$$Nu_{ot} = 0.057\ C_\beta\ \max(Re_{min},\ Re_o)^{0.8}\ Pr^{0.4} \quad \text{for turbulent flow,} \qquad (4.4.2\text{-}20)$$

$$Nu_{ol} = 4 \quad \text{for laminar flow, and} \qquad (4.4.2\text{-}21)$$

$$Re_{min} = 800\ . \qquad (4.4.2\text{-}22)$$

Equation (4.4.2-18) is the experimental formula introduced by Fishirden and Saunders[50]. Equation (4.4.2-20) is also the experimental formula by Watanabe[51].

d_o : Outer diameter of tube
Nu_o : Nusselt number ($= h_{tc} \cdot d_o / k$)
Pr : Prandtle number ($= c_p \cdot \mu / k$)
Re_o : Reynolds number ($= u_o \cdot d_o / \nu$)
u_o : Gap velocity

The gap velocity can be expressed as follows:

$$u_o = \frac{G_o}{\gamma S_a}$$

where

$$S_a = \frac{\pi}{4}(D_o^{b2} - D_i^{b2}) - \sum_{i=1}^{m} \pi D_i^h d_o - S_r - S_o \ .$$

G_o : External flow rate in weight
D_o^b : Outer diameter of tube bundle flow area
D_i^b : Inner diameter of tube bundle flow area
D_i^h : Helix diameter of i-th column
m : Number of helix columns
S_r : Cross sectional area of radiation plates
S_o : Cross sectional area of tube support plats, and other plates

The coefficient C_h is the arrangement factor as a function of tube arrangement, pitch-to-diameter ratio and Reynolds number. The coefficient C_β can be given through the following expression[52].

$$C_\beta = \eta_f \cdot \eta_e \cdot \eta_\theta \cdot \eta_s \cdot \beta \qquad (4.4.2\text{-}23)$$

$\eta_f(\leqq 1)$: factor caused by out-of-round tube bent to be flat
$\eta_e(\leqq 1)$: factor by eccentricity of helically coiled tube from centre between radiation plates
$\eta_\theta(\leqq 1)$: factor by oblique flow to helically coiled tube
$\eta_s(\leqq 1)$: factor by narrow longitudinal pitch of tube
$\beta(\leqq 1)$: factor of heat transfer rate enhanced by effects of radiation plates

These correlations are summarized in Table 4.4.2-1.

Table 4.4.2-1 Heat Transfer Coefficient Package for Helium

Annulus flow channel

$Nu = \max(Nu_l, Nu_t)$

$Nu_l = c(\alpha) (T_b/T_w)^{0.5}$

$c(\alpha) = -4.8268\alpha^3 + 12.7516\alpha^2 - 12.2505\alpha + 9.7170$

$Nu_t = 0.020\alpha^{-0.16} Re^{0.8} Pr^{0.4} (T_b/T_w)^{0.5}$

α : Diameter ratio ($=d_i/d_o$)
De : Equivalent diameter ($=d_o-d_i$)

Circular flow channel

$Nu = \max(Nu_l, Nu_t)$

$Nu_l = 4.36 (T_b/T_w)^{0.5}$
$Nu_t = 0.02 Re^{0.8} Pr^{0.4} (T_b/T_w)^{0.5}$

De : Equivalent diameter ($=d_i$)

Inside tube of baffled shell-and-tube type heat exchanger

$Nu = \max(Nu_l, Nu_t)$

$Nu_l = 4$
$Nu_t = 0.023 Re^{0.8} Pr^{0.4}$

De : Equivalent diameter ($=d_i$)

Outside tube flow of baffled shell-and-tube type heat exchanger

$Nu_o = C_a \max(Re_o, Re_{min})^{0.6} Pr^{1/3} \mu^*$

$Re_{min} = 10.0$

μ^* : Viscosity ratio ($= \mu/\mu_w$)
μ_w : Viscosity at wall temperature T_w
Re_o : Reynolds number ($= u_o d_o/\nu$)
u_o : Weighted velocity ($= Q/A_e$)
A_e : Weighted flow area ($=((A_c)_{Bh} \cdot (A_c)_{cross})^{1/2}$)
$(A_c)_{Bh}$: Baffle-hole area ($= K_{Bh} \cdot \pi/4\ D_s^2$)
$(A_c)_{cross}$: Cross-flow area ($=(D_s - Z_h d_0)\overline{BP}$)
$\overline{BP}$: Distance between baffle plates
D_s : Inside diameter of shell
K_{Bh} : Ratio of baffle-hole area to cross-sectional area of shell
Z_h : Number of tubes at the centre of cross section of shell

Table 4.4.2-1 Heat Transfer Coefficient Package for Helium (Continued)

Inside tube flow of helically-coiled type heat exchanger

$$Nu = \max(Nu_l, Nu_t)$$

$$Nu_l = 4.36\left(\frac{0.148\ Dean^{1/2}}{1 - 1.813\ Dean^{-1/2}}\right)$$

$$Nu_t = 0.0223\ Re^{5/6}\ d_i^{*1/12}\frac{Pr}{(Pr^{0.6} - 0.057)}\left\{1 + \frac{0.0615}{(Re\ d_i^{*2.5})^{1/6}}\right\}$$

d_i^* : Non-dimensional number ($= d_i / Dm$)
De : Equivalent diameter ($= d_i$)
Dm : Average diameter of helical coils
$Dean$: Dean number ($= Re\ d_i^{*1/2}$)

Outside tube flow of helically-coiled type heat exchanger

$$Nu_o = 0.33\ C_h\ Re_o^{0.6}\ Pr^{0.3} \quad \text{for } Re_o \geqq 7000,$$
$$Nu_o = \max(Nu_{ol}, Nu_{ot}) \quad \text{for } Re_o < 7000$$

$$Nu_{ot} = 0.057\ C_\beta \max(Re_{min}, Re_o)^{0.8}\ Pr^{0.4}$$
$$Nu_{ol} = 4$$

$$Re_{min} = 800.$$

Re_o : Reynolds number ($= u_o d_o / \nu$)
u_o : Mean velocity of external flow $= Q / A_e$)
C_h : Arrangement coefficient
C_β : Coefficient
Q : Mean volumetric rate of external flow

Nomenclature in Table 4.4.2-1

c_p : Specific heat
d_i : Tube inner dia. or inner dia. of annulus channel
d_o : Tube outer dia. or outer dia. of annulus channel
D_e : Equivalent diameter
k : Thermal conductivity
Nu : Nusselt number ($= h_{tr}\ k / D_e$)
Nu_o : Nusselt number ($= h_{tr}\ k / d_o$)
Pr : Prandtle number ($= c_p \mu / k$)
Re : Reynolds number ($= D_e u_i / \nu$)
Re_o : Reynolds number ($= d_o u_o / \nu$)
T_b : Bulk temperature
T_w : Wall temperature
u_i : Mean velocity of inner flow
u_o : Reference velocity of external flow, defined in each correlation
μ : Viscosity
ν : Kinetic viscosity

4.4.3 Radiation Heat Transfer between Slabs

In HTGR dynamics analyses, the radiation heat transfer between structual materials becomes important since the temperatures are very high. In the present work, a model to connect the slabs by radiation heat transfer, which are specified by inputs, is implemented. The model applied is to evaluate the heat transfer rate q_{12} from the inner to the surrounding shell in an annulus flow channel. The net heat transfer rate is written as follows:

$$q_{12} = \frac{\sigma A_1 (T_1^4 - T_2^4)}{1/\varepsilon_1 + (A_1/A_2)(1/\varepsilon_2 - 1)} \quad . \tag{4.4.3-1}$$

T_1 : Surface temperature of inner core
T_2 : Surface temperature of surrounding shell
ε_1 : Emissivity at surface of inner core
ε_2 : Emissivity at surface of surrounding shell
A_1 : Surface area of inner core
A_2 : Surface area of surrounding shell
σ : Stefan-Boltzmann constant

4.4.4 Feedback Reactivity

In THYDE-W, the feedback reactivities due to changes in i) fuel temperature and ii) coolant void fraction are modeled. In the case of gas-cooled reactors, the latter is not necessary. In THYDE-HTGR, therefore, it is replaced by the feedback reactivity due to change in moderator temperature, which is important in the cases of graphite-moderated gas-cooled reactor. The total reactivity Γ_{tot} in Eq. (4.2.2-2) is obtained as follows:

$$\Gamma_{tot} = \Gamma_{ex} + \Gamma_F + \Gamma_M \quad , \tag{4.4.4-1}$$

where

$$\Gamma_F = \gamma_F(T_F(t) - T_F(0)) \quad ,$$

and

$$\Gamma_M = \gamma_M(T_M(t)-T_M(0)) \ .$$

T_F : Fuel temperature averaged over whole core

T_M : Moderator temperature averaged over whole core

Γ_{ex} : External reactivity contribution such as control rod insertion

Γ_F : Feedback reactivity due to fuel temperature change

Γ_M : Feedback reactivity due to moderator temperature change

γ_F : Feedback reactivity coefficient to fuel temperature change

γ_M : Feedback reactivity coefficient to moderator temperature change

4.4.5 Steady State Heat Balance Calculation

In the steady state calculation, the mass flux and the specific enthalpy at a certain node in each loop are given as inputs. The heat transfer rate at each heat slab is also given as an input. The heat slabs are categorized to i) core slabs, ii) heat exchanger slabs and iii) the other slabs. The heat transfer rates at the heat slabs in category ii) are adjusted from the input value in order to hold the total heat balance in each loop, keeping the heat transfer rates at the slabs in the categories i) and iii) as inputs.

When both sides of the heat slab are in contact with fluid nodes as in heat exchanger slabs, the heat transfer rate can be determined by solving the steady state thermal conduction equation, because the temperatures of nodes at both sides and and heat transfer coefficients are given. However, such heat transfer rate is usually not consistent with the input value. In THYDE-W, in order to achieve the consistency of the heat transfer rates, the iteration of the steady state calculations are performed. However, it is not always easy to achieve the convergence. In fact, in HTGR calculations, the iteration calculation often did not converge or led to undesirable steady state solution by this method. In THYDE-W, therefore, the heat transfer areas of the heat exchanger slabs are adjusted to avoid the iteration calculation. The heat transfer areas revised during the steady state calculations are used succeeding transient transient calculation. This method has been commonly used in LWR safety analysis codes[21].

5. Assessment calculation of THYDE-HTGR

Assessment calculations have been performed for the experiments conducted at the High Temperature Helium Test Loop operated by IHI under the research and development program of nuclear steelmaking by the Agency of Industrial Science and Technology of the Ministry of International Trades and Industry. The IHX of the Test Loop is the same type as that of HTTR. The primary purpose of the calculations is to assess the capability of THYDE-HTGR to simulate the thermal-hydraulic steady and transient behaviors of the helium/helium intermediate heat exchanger of helically-coiled type. The calculations have been performed for the following typical experiments and an accident:

i) Steady State Test 001
(Steady state at rated power operation)
ii) Transient Tests D001 and D002
(Transients following the step-wise changes in flow rates)
iii) Accident, called EH-TRIP
(Accident induced by unexpected primary electric heater shutoff)

The Test 001 was conducted under the steady state operation at the rated power. The temperature distributions of both primary and secondary heliums along the helix tubes were measured. The purpose of the Test 001 calculation is to assess the predictability of the heat transfer coefficients under steady state conditions.

In the Test D001, the system response following the step-wise decrease in the primary helium flow was measured. In the Test D002, on the other hand, the response following the step-wise decrease in the secondary helium flow was measured. The purpose of the calculations of ii) and iii) is to assess the adequacy of the IHX model including the predictability of the heat transfer correlations under transient conditions.

5.1 Description of Experiments

The schematic drawing of the High Temperature Test Loop is shown in Fig.5.1-1. The test facility of our interest consists of the primary and

secondary loops and the helium/helium intermediate heat exchanger (IHX) of a helically-coiled type. The primary loop consists of the gas and electrical heaters and gas circulator. The secondary loop consists of the steam heater, reducing gas heater, steam generator and gas circulator.

The schematic figure of the IHX is depicted in Fig.5.1-2. The key specifications are shown in Table 5.1.1. The primary helium enters from the bottom and flows up outside the helicall-coiled tubes to the upper plenum, transferring the heat to the secondary helium, and then turns to flow down through the annuli to the exit at the bottom. The secondary helium enters from the top and flows down inside the helical tubes getting the heat. Once the helium is collected in the hot header through the manifold at the bottom, it flows up through the central hot gas duct to the exit at the top.

5.2 Input Model

Figure 5.2-1 shows the nodalization scheme in the present calculation. The system to be analysed are dscretized by totally 75 nodes, 77 junctions and 26 heat slabs. The descriptions of the nodes and slabs are shown in Tables 5.2-1 and 5.2-2. As shown in these tables, the actual heat transfer section is nodalized into 20 nodes for each side and 20 heat slabs. The components except IHX such as the heat source and sink in the primary and secondary loops, respectively, and the gas circulators are considered to be the components to supply boundary conditions. Therefore, the geometrical data of these components are not corresponding to those in the test facility. The heat input to the heat source volume in the primary system was given as an input as atime table. The rotational speeds of the primary and secondary gas circulators were also given as inputs as time tables. In the heat sink volume of the secondary system, the flow path of only the secondary helium was mdeled and the third loop was treated as boundary conditions, where the fluid temperature and the heat transfer coefficient were appropriately set constant.

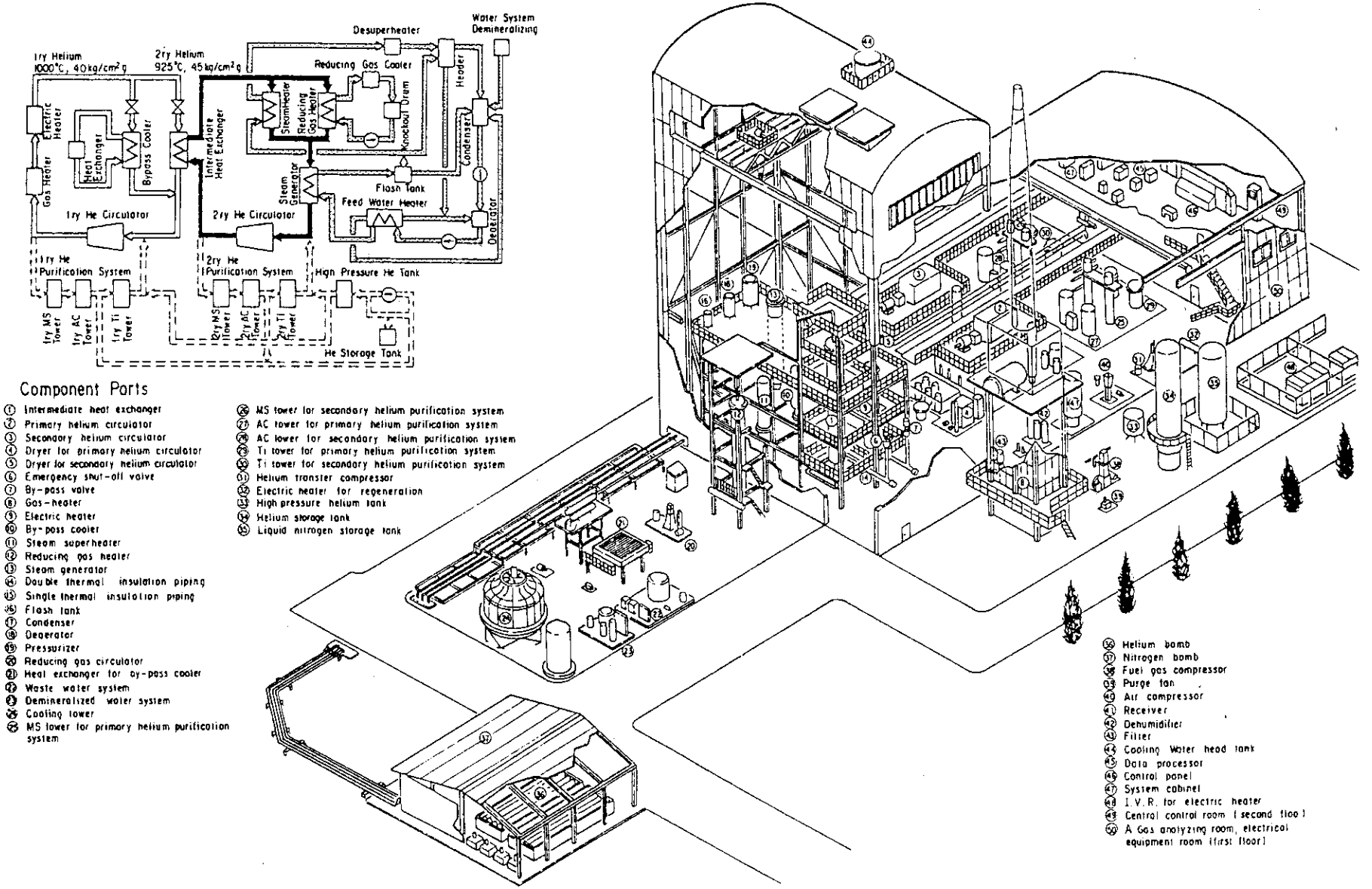

Fig. 5.1-1 Flow Diagram of High Temperature Helium Test Loop in IHI

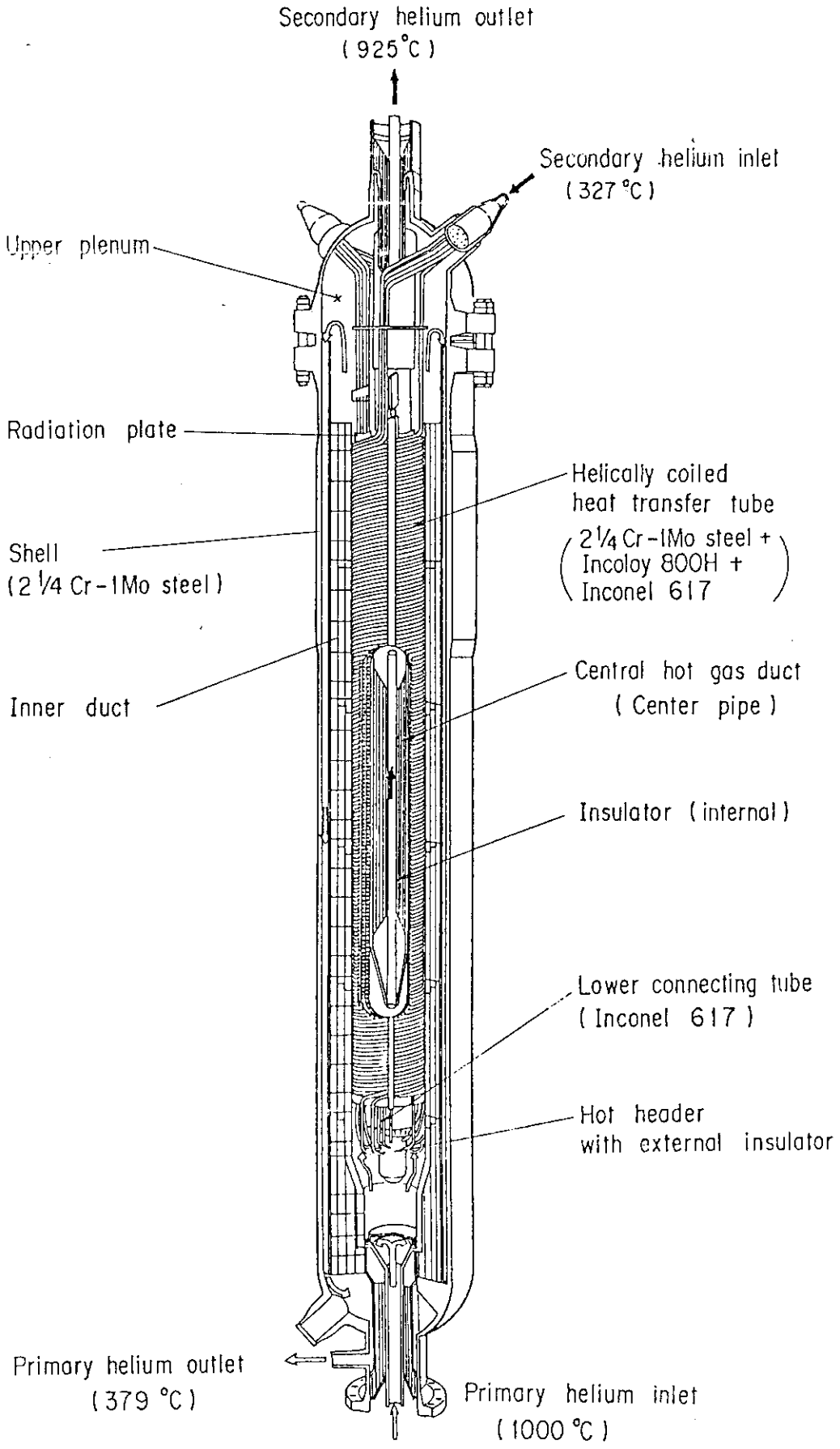

Fig. 5.1-2 Bird's Eye View of ERANS 1.5 MW Intermediate Heat Exchanger

Table 5.1-1 Structural Materials of IHX in ERANS

Component	Material
Tube	Inconel 617 Alloy 800H 2 1/4Cr-1Mo steel
Radiation Plate	Inconel 617 Alloy 800H 2 1/4Cr-1Mo steel
Hot Header	Inconel 617
Central Hot Gas Duct	Inconel 617
Thermal Insulator for High Temperature Service	Kaowool

Table 5.1-2 Major Specification of IHX in ERANS

Items	Specification
Heat Exchanging Rate (Rated Power)	1.5 MW
Number of Heat Transfer Tubes	30
Number of Helical Coil Layers	3
Dimensions of Heat Transfer Tubes	
Outer Diameter	25.4 mm
Wall Thickness	4.0 mm
Tube Pitch	
Radial	45 mm
Axial	40 mm
Tube Length of Effective Heat Transfer Section	36.5 m
Helix Angle	10.45 ℃
Innermost Diameter of Helical Coil	0.60 m
Outermost Diameter of Helical Coil	0.78 m
Height of Effective Heat Transfer Section	6.7 m
Inconel 617	2.7 m
Alloy 800H	1.54 m
2 1/4Cr-1Mo Steel	2.46 m
Wall Thickness of Radiation Plate	6.0 mm
Outer Diameter of IHX	1.55 m

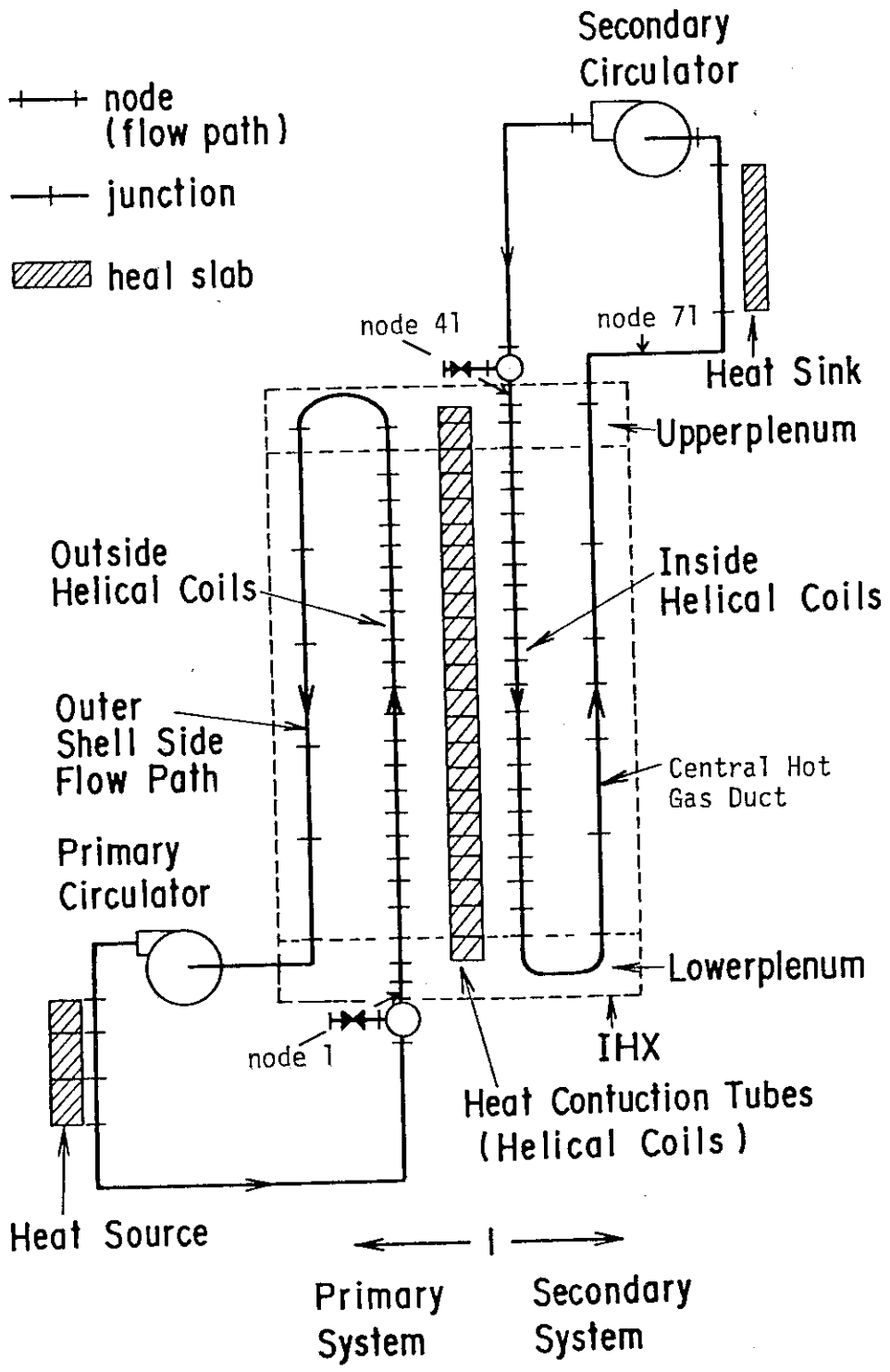

Fig. 5.2-1 Nodalization

Table 5.2-1 Description of Nodes

No. of node	Description
Primary loop	
1	IHX inlet
2-3	Lower plenum
4-23	Outside of helical coil section
24-25	Upper plenum
26-32	Annulus flow path along outside shell
33	Plenum and outlet nozzle
34	Piping connecting IHX and primary gas circulator
35	Primary gas circulator
36	Piping connecting primary gas circulator and heater
37-39	Heater volumes in primary loop
37-39	Piping connecting heater and IHX inlet
41	IHX inlet of secondary loop
Secondary loop	
42-43	Upper plenum
44-63	Inside of helical coil section
64-70	Central hot gas duct
71	Piping connecting IHX outlet and heat sink volume
72	Heat sink volume
73	Piping connecting heat sink volume and secondary gas circulato
74	Piping connecting secondary gas circulator and IHX inlet

Table 5.2-2 Description of Heat Slabs

No. of slab	Description
1-3	Heat source in primary system
4-12	Helically coiled tube wall (Inconel 617)
13-16	Helically coiled tube wall (Alloy 800H)
17-26	Helically coiled tube wall (2 1/4Cr-1Mo Steel)
27	Heat sink in secondary loop

5.3 Calculated Results and Discussions

5.3.1 Steady State Test 001

Figure 5.3.1-1 shows the comparison of temperature profiles along the primary and secondary heliun in IHX between Test 001 and the analysis. As already described in Sec. 4.4.5., the heat transfer rates of the heat slabs in steady state are basically given by inputs, and the heat transfer area in each heat slab specified as a heat exchanger slab is adjusted in the code in order to equate the input heat transfer rate and that calculated by Eq. (4.2.1-2). Therefore, the calculated temperature profiles in Fig. 5.3.1-1 should be considered inputs. Table 5.3.1-1 shows the multiplier in each heat slab, which is multiplied to the heat transfer area in order to obtain the temperature profile shown in Fig.4.4.2-1, along with the heat transfer coefficients at both sides of the slabs. The input heat transfer area is calculated by the geometrical data of the helically-coiled tubes. If it is assumed that the input heat transfer areas are well corresponding to the actual values, the reasons why the multiplier of the heat transfer area deviates from one are mainly as follows: i) the underestimation of the temperature difference between the primary and secondary coolants due to the definition of the bulk temperature explained in Fig.4.2.1-2, and ii) the difference beteen the heat transfer coefficients estimated by an empirical correlation implemented in THYDE-HTGR and actual one. In the present case, the underestimation of the temperature difference due to the definition of the bulk temperature in THYDE-HTGR described in i) is about 30 ℃ because the temperature decrease and increase per one node in the primary and secondary systems, respectively, are approximately 30 ℃. This underestimation gives the values from 1.6 to 1.8 for the multipliers of the heat transfer areas since the temperature difference between the primary and secondary heliums is approximately 70 to 80 ℃. As shown in Table 5.3.1-1, the values of the multipliers obtained as a result of the steady state calculation are similar to these values, and therefore, the fact imples that the heat transfer coefficients are in agreement with the experimental data.

5.3.2 Transient Test D001

In this test, the primary loop flow is suddenly decreased by 5.6 % and the subsequent system response was measured. In this case, the total heat transfer rate at the IHX is decreased and therefore the primary outlet temperature tends to increase and the secondary outlet temperature tends to decrease. In the analysis, first of all, an steady state calculation was performed to simulate the experimental initial conditions. The calculated steady state conditions are compared with the experimental initial conditions in Table 5.3.2-1. Starting from the steady state, the system transient followed by the sudden reduction of the primary flow was simulated. The sudden reduction of the primary flow was realized in the calculation by suddenly reducing the rotational speed of the primary gas circulator. The heat input to the heat source volume in the primary system and the rotational speed of the secondary gas circulator were kept constant. The heat removal from the secondary system heat sink volume was calculated according to the transient of the secondary helium in the code. The calculated results are shown in Figs.5.3.2-1 to 5.3.2-3 along with the experimental data. As shown in Fig.5.3.2-1, the primary flow is overestimated, because the decrease in the primary loop flow is simply simulated by the step-wise reduction of the rotational speed of the primary gas circulator due to lack of information on the operation condition of the gas circulator such as on the control systems applied in the experiment. Figure 5.3.2-2 shows the primary inlet temperatures in both experiment and calculation. In the present calculation, the primary inlet temperature was assumed to be constant and this assumption was realized that the primary loop volume except IHX was taken to be large. It is because the detailed information on the components in the primary system except IHX was not available. This figure shows that this assumption is suitable since the temperature deviates only about 0.5%. Figure 5.3.2-3 shows the calculated secondary outlet temperature along with the experimental data. As shown in the figure, the temperature transient at the secondary outlet is in good agreement with the experimatal data. The experimental data on the primary outlet temperature were not available.

5.3.3 Transient Test D002

In this test, the secondary loop flow is suddenly decreased by 5.6 % and the system response was measured. In this case also, the total heat transfer rate decreases. The procedure of the analysis was similar to that in the analysis of Test D001. The initial conditions in both experiment and calculation are shown in Table 5.3.3-1. The sudden reduction of the secondary flow is realized in the calculation by step-wise reduction of the rotational speed of the secondary gas circulator. The heat input to the heat source volume in the primary system and the rotational speed of the primary gas circulator were kept constant. The heat removal from the secondary system heat sink volume was calculated according to the transient of the secondary helium in the code. The calculated results are shown in Figs.5.3.3-1 to 5.3.3-3 along with the experimental data. In this case, it was more successful to simulate the initial event, i.e. the transient of the secondary flow, as shown in Fig.5.3.3-1, than in the previous case. The primary flow was also almost constant in both experiment and calculation. The primary inlet temperature is almost constant as shown in Fig.5.3.3-2. The secondary outlet temperature, which is the focal point, is shown in Fig.5.3.3-3. In the calculation, although the temperature increase was overestimated, the overall trend was well simulated.

5.3.4 Accident EII-TRIP

In this transient, the electric power of the primary loop was shutdown due to a short circuit. In this case also, the total heat transfer rates at IHX decrease due to the decrease in the primary inlet temperature. In the analysis, starting from the steady state condition, the system transient follwed by the loss-of-primary power was simulated. The rotational speeds of the primary and secondary gas circulators were kept constant during the transient. The loss-of-primary power was simulated by reducing the power of the heat source in the primary system, whose location is denoted by "heat source" in Fig.5.2-1. The power transient was adjusted through the sensitivity calculations so that the primary inlet temperature is in agreement with the experimental data. Figure 5.3.4-1 shows the resultant primary inlet temperature transient along with the experimental data. It was rather difficult to obtain good agreement with the experimental data by only changing the power transient. Figures 5.3.4-2 and 5.3.4-3 show

the transients of the primary and secondary mass flow rates, respectively. The maximum deviation from the experimental data is about 8%. Figures 5.3.4-4 shows the secondary inlet temperature. The maximum deviation from the experimental data is about 2%. The reason for these deviations is that the characteristics of the components such as the circulators and the steam generator could not be modeled realistically due to lack of experimental information. Figure 5.3.4-5 shows the secondary outlet temperature, which is the focal point in this analysis. Although the temperature is underestimated at maximum about 8%, the experimental trend was well simulated.

It is noted that the experimental curves shown in Figs.5.3.4-1 to 5.3.4-5 are obtained by smoothly interpolating the measured data, whose measurment frequency was 30 minutes.

Table 5.3.1-1 Calculated Multipliers to Heat Transfer Areas

Slab No.	Heat transfer coef. (kcal/s·m²·℃)		Multiplier to Heat transfer area
	Secondary	Primary	
5	0.381	0.0563	1.130
6	0.381	0.0561	1.931
7	0.380	0.0560	1.900
8	0.379	0.0558	1.870
9	0.378	0.0557	1.842
10	0.377	0.0555	1.815
11	0.376	0.0553	1.789
12	0.375	0.0552	1.764
13	0.373	0.0550	1.739
14	0.372	0.0547	1.717
15	0.370	0.0545	1.696
16	0.369	0.0543	1.676
17	0.367	0.0541	1.621
18	0.365	0.0538	1.606
19	0.364	0.0536	1.591
20	0.362	0.0533	1.578
21	0.360	0.0530	1.565
22	0.358	0.0527	1.553
23	0.356	0.0524	1.542
24	0.354	0.0523	1.039

Table 5.3.1-2 Results of Steady State Test 001

Parameter	Experiment	Calculation
Flow Rate (kg/s)		
Primary helium	0.4822	0.4822
Secondary helium	0.4961	0.4903
Helium Temperature (°C)		
Primary		
inlet helium	1000.0	1000.0
outlet helium	372.	389.5
Secondary		
inlet helium	323.	322.3
outlet helium	917.	916.7
Helium Pressure (kgf/cm^2g)		
Primary		
inlet	39.8	39.8
outlet	39.4	39.2
Secondary		
inlet	45.7	45.7
outlet	44.7	44.7

Table 5.3.2-1 Initial Conditions in Test D001

Parameter	Experiment	Calculation
Flow Rate (kg/s)		
Primary helium	0.4994	0.4995
Secondary helium	0.4883	0.4993
Helium Temperature (°C)		
Primary		
inlet helium	907.5	907.5
outlet helium	-	388.9
Secondary		
inlet helium	314.0	314.0
outlet helium	844.4	844.4
Helium Pressure (kgf/cm^2g)		
Primary		
inlet	38.0	37.5
outlet	-	36.9
Secondary		
inlet	-	44.5
outlet	42.5	43.6

Table 5.3.3-1 Initial Conditions in Test D002

Parameter	Experiment	Calculation
Flow Rate (kg/s)		
Primary helium	0.5	0.4995
Secondary helium	0.4885	0.4993
Helium Temperature (°C)		
Primary		
inlet helium	908.0	907.5
outlet helium	-	388.9
Secondary		
inlet helium	-	314.0
outlet helium	844.8	844.4
Helium Pressure (kgf/cm^2g)		
Primary		
inlet	38.0	37.5
outlet	-	36.9
Secondary		
inlet	-	44.5
outlet	42.55	43.6

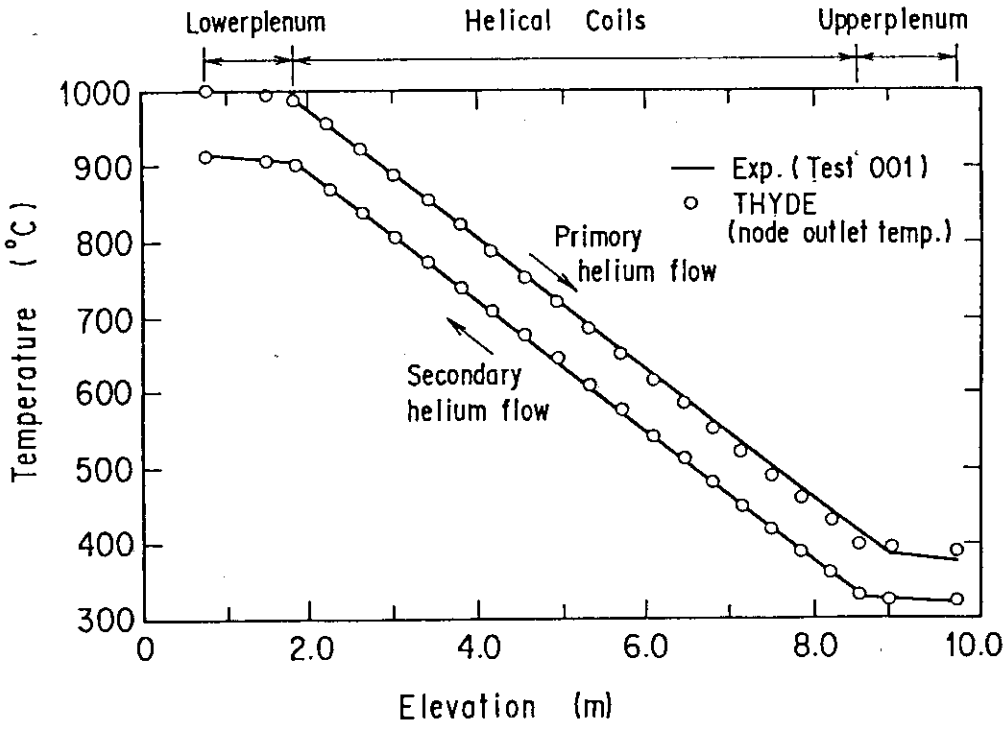

Fig. 5.3.1-1 Helium Temperature Profile in Test 001

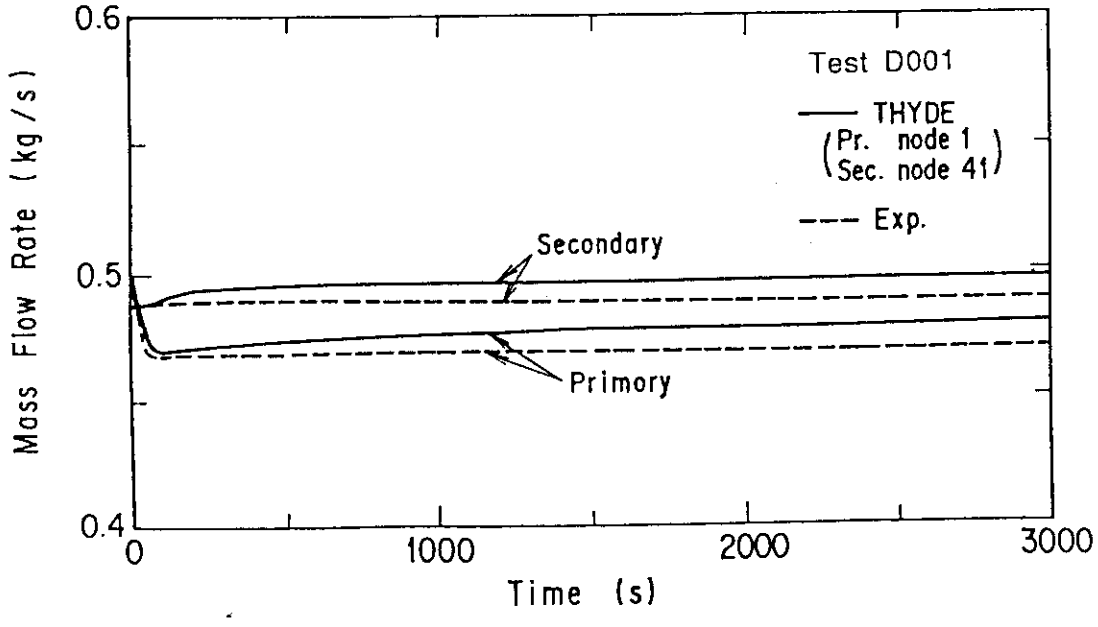

Fig. 5.3.2-1 Transients of Primary and Secondary Flows in Test D001

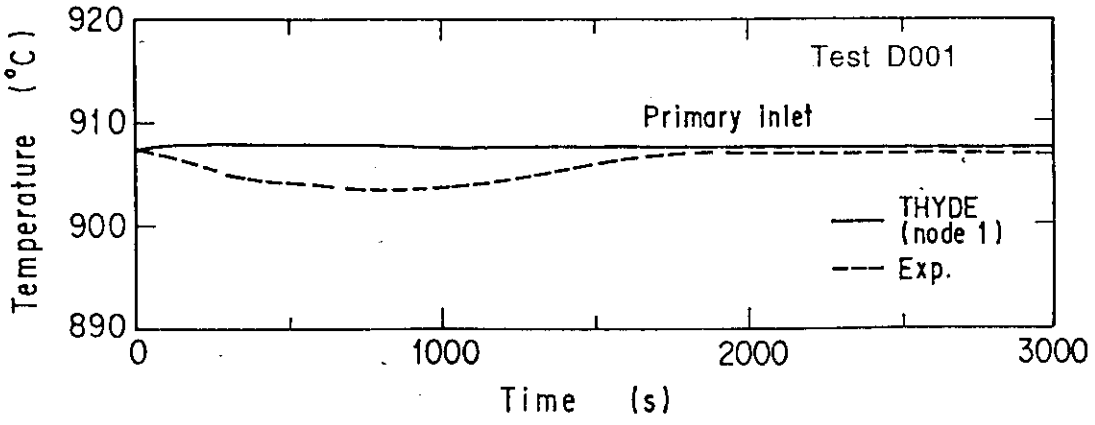

Fig. 5.3.2-2 Transient of Primary Inlet Temperature in Test D001

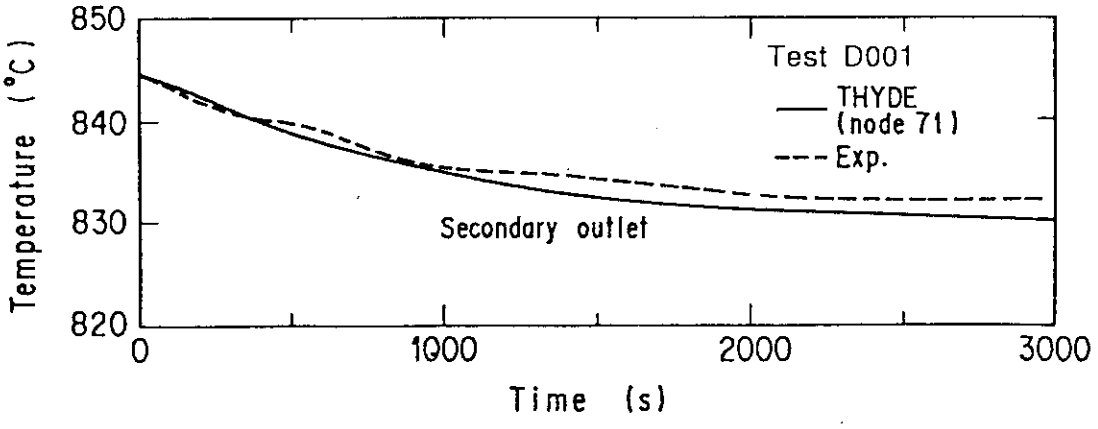

Fig. 5.3.2-3 Transient of Secondary Outlet Temperature in Test D001

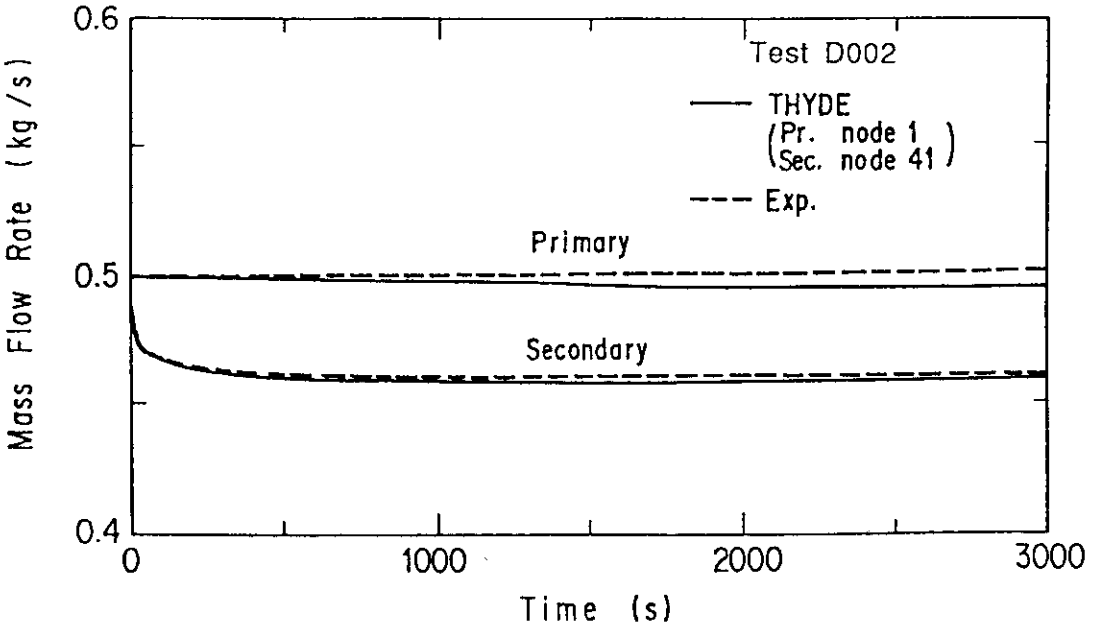

Fig. 5.3.3-1 Transients of Primary and Secondary Flows in Test D002.....

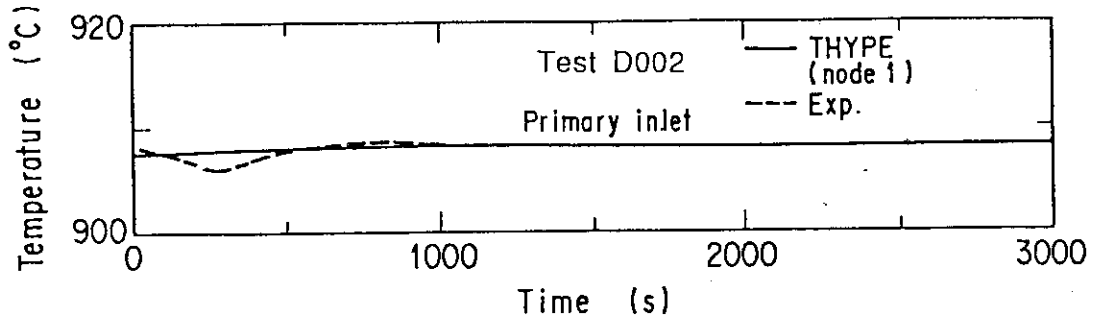

Fig. 5.3.3-2 Transient of Primary Inlet Temperature in Test D002

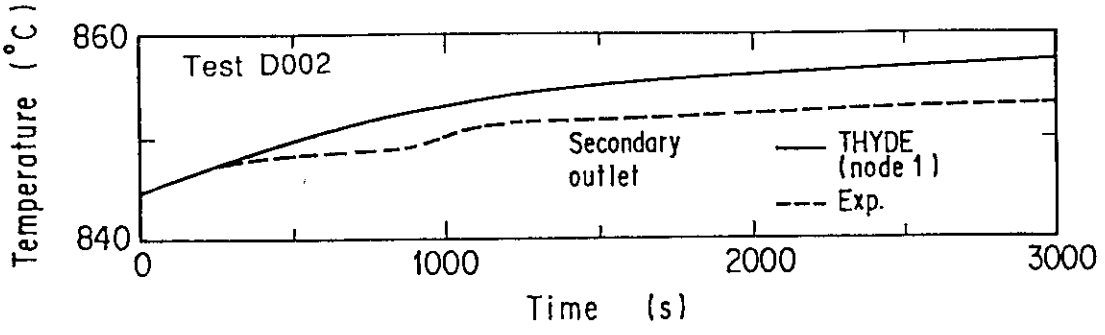

Fig. 5.3.3-3 Transient of Secondary Outlet Temperature in Test D002

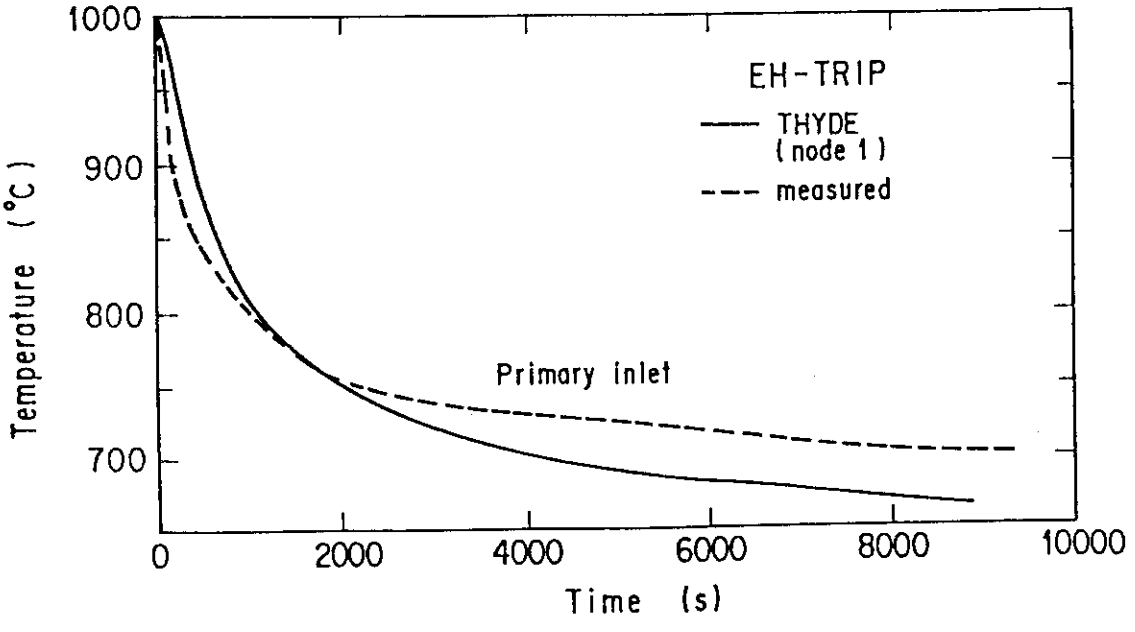

Fig. 5.3.4-1 Transient of Primary Inlet Temperature in EH-TRIP

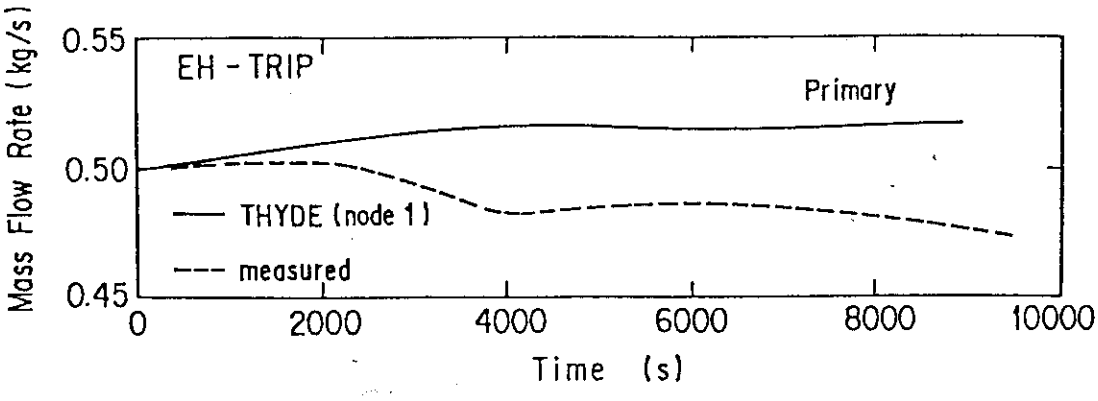

Fig. 5.3.4-2 Transient of Primary Flow in EH-TRIP

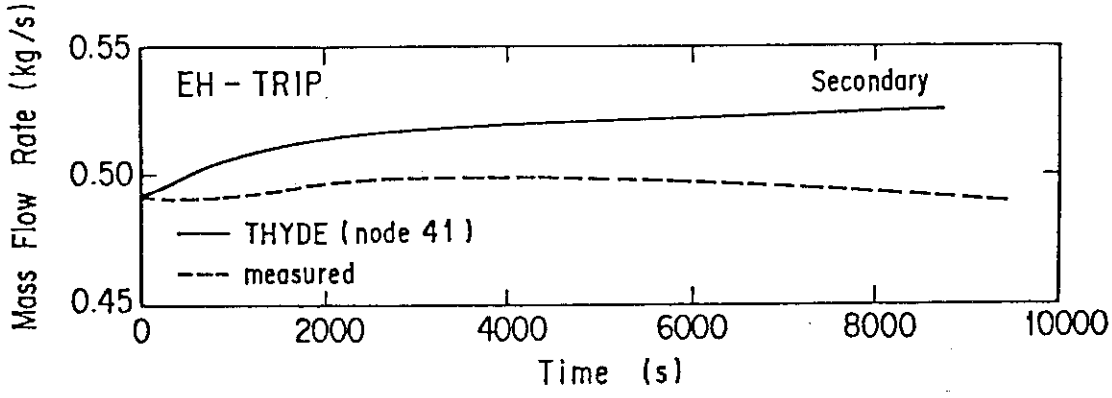

Fig. 5.3.4-3 Transient of Secondary Flow in EH-TRIP

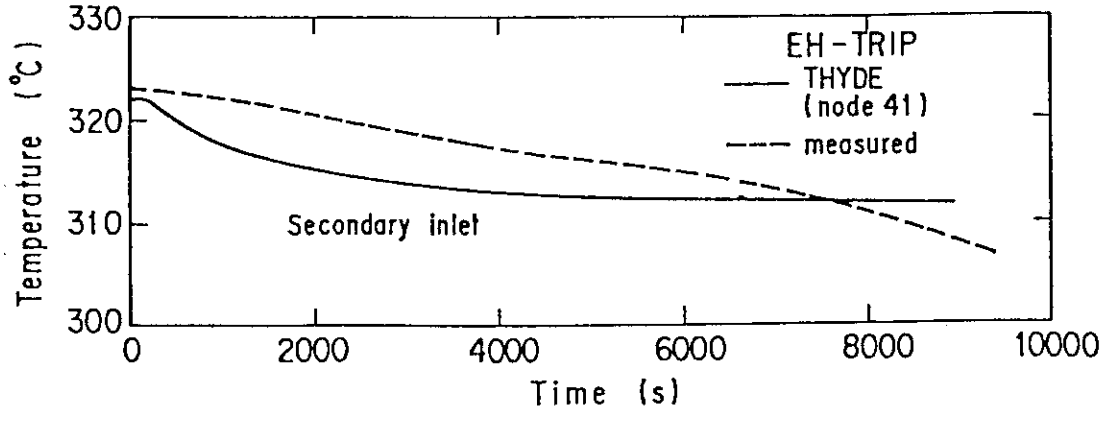

Fig. 5.3.4-4 Transient of Secondary Inlet Temperature in EH-TRIP

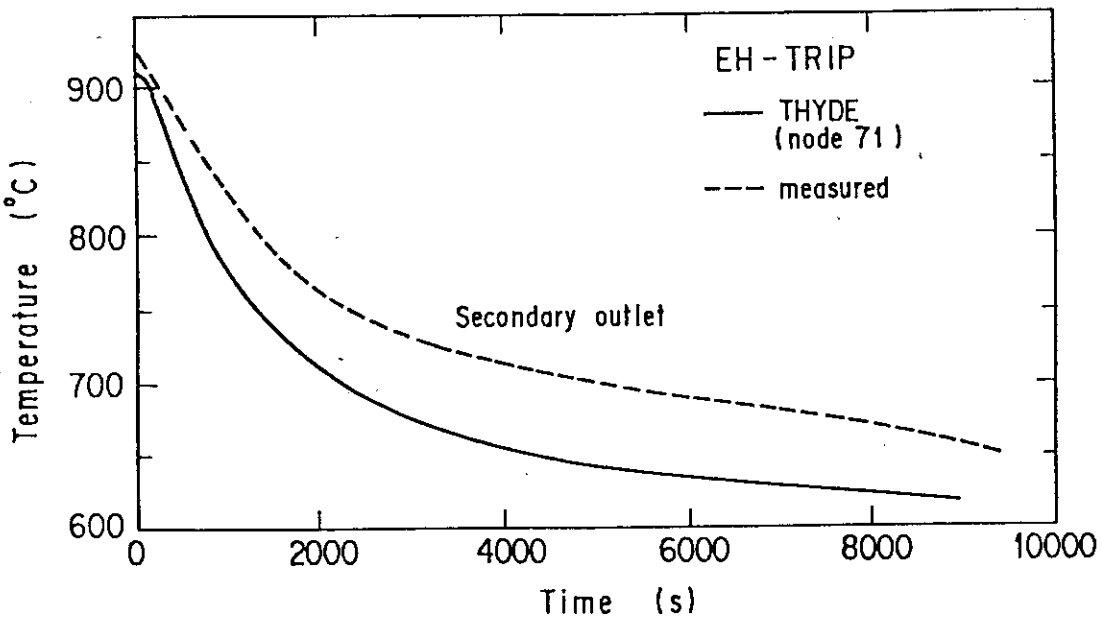

Fig. 5.3.4-5 Transient of Secondary Outlet Temperature in EH-TRIP

6. Concluding Remarks

The THYDE-HTGR code has been successfully developed for transient thermal-hydraulic analyses of HTGRs, based on the THYDE-W code for LWR transient analyses. The major code upgrading is to treat helium loops as well as water loops. The models and method applied in THYDE-HTGR have been assessed through the analyses of the experiments at the High Temperature Helium Test Loop conducted by IHI. The major models which have been assessed through the present experiment analyses are the basic thermal-hydraulic models to solve the conservation equations including its numerics and the model for the helium/helium intermediate heat exchanger. The calculated results are shown to be in good agreement with the experimental data, and therefore, the applicability of THYDE-HTGR to HTGRs has been assessed within the scope of the present experiment analyses.

Acknowledgements

The authors wish to express their gratitude to Dr. S. Saito, Diputy Director, Department of HTTR Project, and Mr. T. Tanaka, Head, HTTR Development Division, Department of HTTR Project, for their encouragements and valuable suggestions. Thanks are also due to Dr. Y. Sudo, Head, Project Management Division, Department of HTTR Project, and Mr. Y. Miyamoto, Head, HENDEL Development Laboratory, Department of High temperature Engineering, for their willingness to help in the course of this work. Appreciation is also due to Dr. Y. Asahi, Reactor system Laboratory, Department of Reactor Engineering, for his constructive comments and suggestions in the early stage of this work. Calculations given in Sect.5 are based on the experimental data on the plant dynamics simulation tests and an accident by the High-Temperature Helium Test Loop. The authors also would like to thank the office for National Research and Development Program of the Agency of Industrial Science and Technology for approving the publication of this report.

6. Concluding Remarks

The THYDE-HTGR code has been successfully developed for transient thermal-hydraulic analyses of HTGRs, based on the THYDE-W code for LWR transient analyses. The major code upgrading is to treat helium loops as well as water loops. The models and method applied in THYDE-HTGR have been assessed through the analyses of the experiments at the High Temperature Helium Test Loop conducted by IHI. The major models which have been assessed through the present experiment analyses are the basic thermal-hydraulic models to solve the conservation equations including its numerics and the model for the helium/helium intermediate heat exchanger. The calculated results are shown to be in good agreement with the experimental data, and therefore, the applicability of THYDE-HTGR to HTGRs has been assessed within the scope of the present experiment analyses.

Acknowledgements

The authors wish to express their gratitude to Dr. S. Saito, Diputy Director, Department of HTTR Project, and Mr. T. Tanaka, Head, HTTR Development Division, Department of HTTR Project, for their encouragements and valuable suggestions. Thanks are also due to Dr. Y. Sudo, Head, Project Management Division, Department of HTTR Project, and Mr. Y. Miyamoto, Head, HENDEL Development Laboratory, Department of High temperature Engineering, for their willingness to help in the course of this work. Appreciation is also due to Dr. Y. Asahi, Reactor system Laboratory, Department of Reactor Engineering, for his constructive comments and suggestions in the early stage of this work. Calculations given in Sect.5 are based on the experimental data on the plant dynamics simulation tests and an accident by the High-Temperature Helium Test Loop. The authors also would like to thank the office for National Research and Development Program of the Agency of Industrial Science and Technology for approving the publication of this report.

References

1. Japan Atomic Energy Research Institute, :Present status of HTGR research & development, (1988).

2. Ohashi, K. et al.: Development of HTGR plant dynamics simulation code, FAPIG(the First Atomic Power Industry Group), (in Japanese), Vol. 116, (1987).

3. ASAHI, Y.: Description of THYDE-P code (Preliminary report of methods and models, JAERI-M7751, (1978).

4. ASAHI, Y.: User's manual for THYDE-P1, JAERI-M 82-38, (1982).

5. ASAHI, Y., HIRANO, M. and SATO, K., : THYDE-P2: RCS(Reactor-Coolant System) Analysis Code, JAERI 1300, (1986).

6. ASAHI, Y., HIRANO, M. : Verification study of LOCA analysis code THYDE-P (Sample calculation run 10), JAERI-M8560, (1979).

7. HIRANO, M., ASAHI, Y.: Through analysis of LOFT L2-2 by THYDE-P code 1 (Sample calculation run 30), JAERI-M9535, (1981).

8. HIRANO, M.: Through analysis of LOFT L2-3 by THYDE-P code (Sample calculation run 40), JAERI-M9765, (1981).

9. SHIMIZU, T., ASAHI, Y.: Through calculation of 1.100MWe PWR large break LOCA by THYDE-P (Sample calculation run 20), JAERI-M9818, (1981).

10. HIRANO, M.: Analysis of LOFT small break experiment L3-1 with THYDE-P code (CSNI international standard problem No. 9 and THYDE-P sample calculation run 50), JAERI-M82-008, (1982).

11. HIRANO, M.: Analysis of LOFT L3-6/L8-1 with THYDE-P (CSNI international standard problem No. 11 and THYDE-P sample calculation run 60), JAERI-M82-028, (1982).

12. KOSUGI, S. et al.: Analysis of PKL test K9 by THYDE-P code (CSNI ISP No. 10 and THYDE-P sample calculation run 70), JAERI-M82-115, (1982).

13. KANAZAWA, M. et al.: A through calculation of 1,100 MWe PWR large break LOCA by THYDE-P1 EM model, JAERI-M 84-132, (1984).

14. HIRANO, M. and AKIMOTO, M., "Pre-Test Prediction of FIX-II Intermediate Break Experiment with THYDE-P1", JAERI M 85-115, (1985).

15. ASAHI, Y. and SUZUKI, Y., : New non-equilibrium thermal-hydraulic model (I), Theory, J. Nucl. Sci. Technol, 21(9), 657, (1984).

16. ASAHI, Y. and ASAKA, H., : New non-equilibrium thermal-hydraulic model (II), Application to LOFT L2-3, J. Nucl. Sci. Technol, 21(10), 753, (1984).

17. ASAHI, Y., ARAYA, F. and WATANABE, T., : Evaluation of PWR-LOCA under LOFT L2-3 condition, J. Nucl. Sci. Technol, 24(5), 365, (1987).

18. REEDER, D. L.: LOFT system and test description (5.5ft corel LOCES), NUREG/CR-0247, (1978).

19. HIRANO, M. and SUDO, Y., :Analytical study on thermal-hydraulic behavior of transient from forced circulation to natural circulation in JRR-3, J. Nucl. Sci. Technol, 23(4), 352, (1986).

20. MOORE, K. V., :RELAP4 -A computer program for transient thermal-hydraulic analysis, ANCR-1127, Dec. 1973.

21. TRAC-PF1:An Advanced best estimate computer program for pressurized water reactor analysis," NUREG/CR-3567, LA-9944-MS (1984).

22. Ransom, V. H., et al. : RELAP5/MOD1 code description, NUREG/CR-1826, EGG-2070 (1982).

23. UKIKUSA, H., et al. :Design, onstuction and operation experience of He-He intermediate heat exchanger, presented at the Japan-U. S. Heat Transfer Joint Seminar, Tokyo, Japan, held on Sept.29 - Oct.2, 1980.

24. SHURE, K., :Fission product decay energy, WAPD-BT-24, Dec., (1961).

25. American national standard ANSI/ANS-5.1, (1979).

26. ZUBER, N., FINDLAY, J.A.: Average volumetric concentrations in two-phase flow systems, J. Heat Trans. 87, 453, (1965).

27. BIASI, L., etal.: Studies on burnout: Part 3, Energia Nucleare, (1967).

28. SLIFER, B. C., etal.: Loss-of-coolant accident and emergency core cooling methods for general electric boiling water reactor, NEDO-10329, General Electric Company, Equation C-32, (1971).

29. ZUBER, N., et al.: The hydrodynamic crisis in pool boiling of saturated and subcooled liquids, International Developments in Heat Transfer, Part II, pp 230-236, (1961).

30. DITTUS, F. W, BOELTER, L. M. K.: Heat transfer in automobile Radiators of the tubelar tube, 2, No. 13, pp.334-461, (1930).

31. JENS, W. H. and LOTTES, :Analysis of heat transfer, burnout, pressure drop for high pressure water, ANL-4627, (1951).

32. THOM, J. R. S., et al.: Boiling in subcooled water during flow up heated tube or annuli, Proc. Instn. Mech. Engrs., Vol 1801 Part 3C, pp 226-246, (1966).

33. MCADAMS, W. H., :Heat transmission, 3rd Ed., p.337, McGraw-Hill, New York, (1954).

34. BORDELON, F. M., et al., ;LOCTA-IV program: loss-of-coolant transient analysis, WCAP-8305, (1974).

35. MCELIGOT, D. M., et al., J. Trans. Amer. Soc. Mech. Engrs., 88, Series C, pp 239-245, (1966).

36. GROENEVELT, D. C.: An investigation of heat transfer in the liquid

deficient regime, Report AECL-3281, Chalk Rever, Ontario, (1968).

37. DOUGAL, R. L., ROHSENOW, W. M.: Film boiling on the inside of vertical tubes with flow of the fluid at low qualities, MIT-TR-9079-26, (1963).

38. BERENSON, P. J., :Film-boiling heat transfer R from a horizontal surface, J. of Heat Transfer, Vol. 83, pp 351-358, Aug. (1961).

39. BROMLEY, L.A., et al.: Heat transfer in forced convection film boiling, Ind. Eng., Chem, 45, 2619, (1953).

40. POMERALTZE: Film boiling on a horizontal tube in increased gravity fields, J of Heat Transfer, 86, pp 213-219, (1964).

41. MOODY, F. J.: Maximum flow rate of single phase ans two-phase mixture, Heat Trans.-Trans. ASME, 87nl, pp134-142, (1965)

42. ZALOUDEK, F. R.: Steam water critical flow from high pressure system, HW-63936, Hanford work, (1967).

44. SUZUKI, K. et al.,: Core Thermal design of the experimental VHTR detailed design stage II, JAERI-M 85-187, (1985)

45. Private Communication with S. Maruyama

46. GA-A 12985

47. DONOHUE, D. A.: Heat transfer and pressure drop in heat exchangers, Ind. Engng. Chem., Vol. 41, Non. 11, (1949).

48. MORI, Y and WATANABE, K.: J. of JSME (in Japanese), Vol. 45, No. 397, pp. 1343-1353, (Sept., 1979).

49. HADA, K, Private communication with K. Watanabe, (1979).

50. FISHIRDEN, M and SAUNDERS, O. A.,: Introduction to heat transfer, Oxford Clarendon Press, p132, (1950).

51. WATANABE, K., Ph.D. Thesis, (1980).

52. MORI, M et al.: Design and thermal dynamic analyses on the intermediate heat transfer for HTGR, Int. Center for Heat and Mass Transfer XVII Int. Symposium for High Temperature Heat Exchangers, Dubrounik, Yugoslavia, Aug. (1985).

Appendix Properties of Helium and Structural Materials

In this appendix, the property data implemented in THYDE-HTGR are summarized. The properties of helium are used as the state equations for the conservation equations and for the other constitutive models such as wall friction, heat transfer coefficient, etc. The property data of the structural material are used for the heat slab model.

A.1 Properties of Helium

The physical properties of helium implemented in the present work are shown in Table A.1-1. The density ρ is given as as a third order polinomial function of temperature T in K. The solution procedure to obtain ρ as a function of specific enthalpy h ($= c_pT$) is shown as follows:

$$\rho = \left(\frac{-\beta_2+(\beta_2^2+4\beta_1^3)^{1/2}}{2}\right)^{1/3} + \left(\frac{-\beta_2-(\beta_2^2+4\beta_1^3)^{1/2}}{2}\right)^{1/3} - \frac{a_1}{3a_0} , \qquad (A.1\text{-}1)$$

where

$$\beta_1 = -\frac{a_1^2}{9a_0^2} + \frac{a_2}{3a_0} ,$$

$$\beta_2 = \frac{2a_1^3}{27a_0^3} - \frac{a_1a_2}{3a_0^2} + \frac{a_3}{a_0} ,$$

$$a_0 = C(T) ,$$

$$a_1 = B(T) ,$$

$$a_2 = 1 ,$$

and

$$a_3 = -\frac{P}{RT} .$$

The differential values to be used for the Jacobian matrix are obtained as follows:

$$\left(\frac{\partial \rho}{\partial P}\right)_h = -\frac{c_p}{Rh} , \qquad (A.1\text{-}2)$$

and $(\partial\rho/\partial h)_P$ is obtained by numerical differenciation.

Table A.1-1 Physical Properties of Helium[6]

Properties	Formula
Density ρ (kg/m^3)	$\rho = P/RT - \rho^2 B(T) - \rho^3 C(T)$ $B(T) = 4.5 \cdot 10^{-4} + 5.42/(1890 + T)$ $C(T) = 1.7 \cdot 10^{-7} + 4.2 \cdot 10^{-3}/(1890 + T) + 25.3/(1890 + T)^2$
Specific heat capacity c_p $(J/kg \cdot K)$	$c_p = 5/2\ R$ $= 5.193 \cdot 10^3$ $(= 1.240\ kcal/kg \cdot K)$
Thermal conductivity k $(J/m \cdot s \cdot K)$	$k = k_0$ for $P < 10^5\ Pa$ $k = k_0 + 2.33 \cdot 10^{-4}\rho + 2.39 \cdot 10^{-6}\rho^2$ for $P \geq 10^5\ Pa$ $k_0 = 2.97 \cdot 10^{-3}\ T^{0.69} + \dfrac{9.23 \cdot 10^9 (T - 273.16)}{(T - 273.16)^5 + 4.29 \cdot 10^{14}}$
Viscosity μ $(N \cdot s/m^2)$	$\mu = \mu_0$ for $P < 10^5\ Pa$ $\mu = \mu_0 + 2.67 \cdot 10^{-10}\ \rho^2$ for $P \geq 10^5\ Pa$ $\mu_0 = 3.78 \cdot 10^{-7} T^{0.69} + \dfrac{5 \cdot 10^{-7}}{0.52 + T/569.6}$

$R = 2.0772 \cdot 10^3$ $(Pa \cdot m^3/kgm \cdot K)$

T : Temperature in K

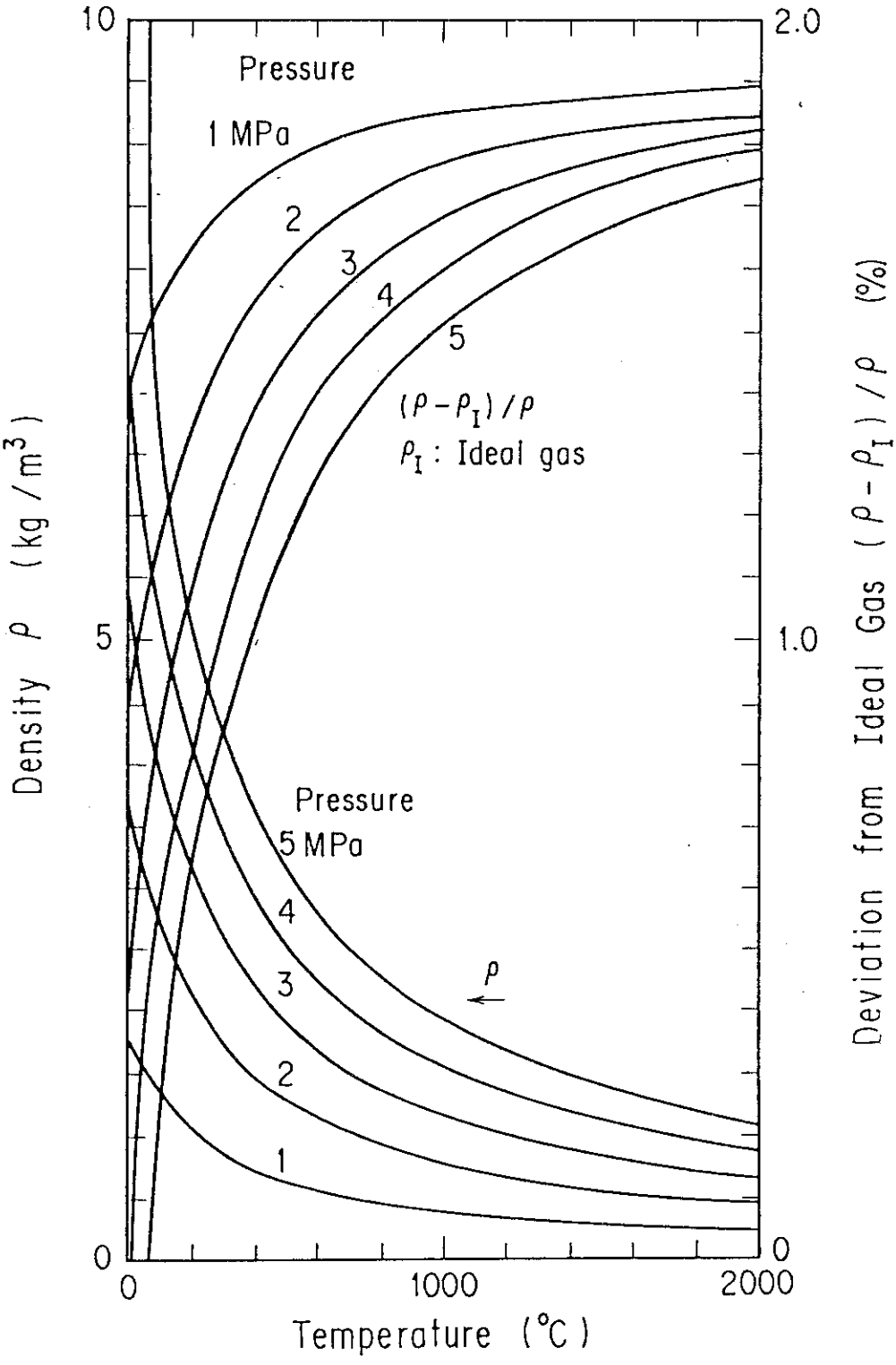

Fig. A.1-1 Density of Helium

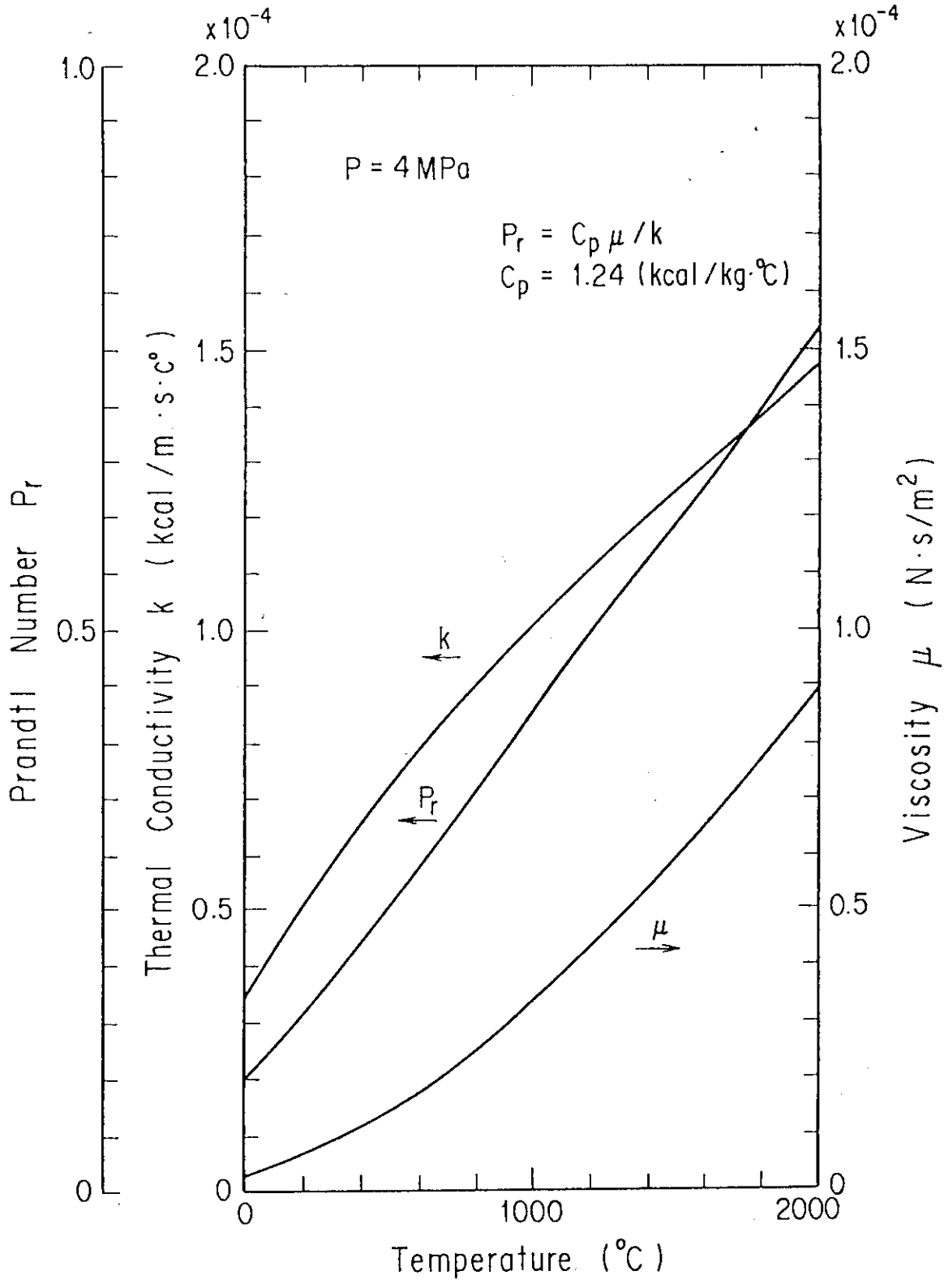

Fig. A.1-2 Physical Properties of Helium

A.2 Properties of Structual Materials

The property data of totally 9 kinds of structual materials, which are often used in HTGR, are implemented. These materials are as follows:

(1) Fuel compact
(2) Graphite IG 110
(3) Graphite PGX
(4) Carbon block ASR-0RB
(5) Alloy 800H
(6) 2 1/4 Cr-1 Mo steel
(7) Hastelloy XR
(8) SUS 304
(9) Thermal insulator for low temperature service
(Calcium Silicate Heat Insulating Material)

The property data for these materials are shown as follows:

(1) Fuel compact[1]

Specific weight:

$\gamma = 2.46 \ (g/cm^3)$.

Specific heat:

$$c_p = 0.115689 + 5.38719 \cdot 10^{-4} T - 6.27977 \cdot 10^{-7} T^2 + 3.82411 \cdot 10^{-10} T^3 - 1.12556 \cdot 10^{-13} T^4 + 1.27705 \cdot 10^{-17} T^5 \quad (cal/g \cdot ℃) ,$$

where T is the temperature in ℃.

Thermal conductivity:

$k = 0.03 \ (cal/cm \cdot s \cdot ℃)$.

(2) Graphite IG-110[1]

Specific weght:

$\gamma = 1.75 (g/cm^3)$.

Specific heat:

$$c_p = 0.54212 - 2.42667 \cdot 10^{-6} T - 90.2725 T^{-1} - 4.34493 \cdot 10^{4} T^{-2} + 1.59309 \cdot 10^{7} T^{-3} - 1.43688 \cdot 10^{9} T^{-4} \quad (kcal/g \cdot ℃) ,$$

where T is the absolute temperature in K, $T < 3000$.

Thermal conductivity:

$$k = k_0(T)\ f_0^k(T) \quad (cal/cm \cdot s \cdot ℃)$$

$$k_0(T) = k_0(T=20℃)\ f(T)$$

$$k_0(T=20℃) = 0.30 \quad (cal/cm \cdot s \cdot ℃)$$

$$f(T) = 1.02748 - 1.35887 \cdot 10^{-3}\ T + 1.11271 \cdot 10^{-6}\ T^2 - 4.76484 \cdot 10^{-10}\ T^3 + 8.69490 \cdot 10^{-14}\ T^4$$

where T is the temperature in ℃, $20℃ \leqq T \leqq 1800℃$.

(3) Graphite PGX[2]

Specific weight:

$$\gamma = 1.74 \quad (g/cm^3) .$$

Specific heat:

$$c_p = 0.54212 - 2.42667 \cdot 10^{-6}\ T - 90.2725\ T^{-1} - 4.34493 \cdot 10^4\ T^{-2} + 1.59309 \cdot 10^7\ T^{-3} - 1.43688 \cdot 10^9\ T^{-4} \quad (kcal/g \cdot ℃) ,$$

where T is the absolute temperature in K. Thermal conductivity:

$$k = 0.26\ f_R(T) \quad (cal/cm \cdot s \cdot ℃) ,$$

where

$$f_R = 1.02264 - 1.2099 \cdot 10^{-3}\ (T-273.16) + 9.43534 \cdot 10^{-7}\ (T-273.16)^2 - 4.36017 \cdot 10^{-10}\ (T-273.16)^3 + 9.49132\ 10^{-14} \cdot (T-273.16)^4 ,$$

and T is the absolute temperature in K, $20 \geqq T-273.16 \geqq 1600$.

(4) Carbon block ASR-0RB

Specific weight:

$$\gamma = 1.68 \quad (g/cm^3) .$$

Specific heat:

$$c_p = 0.54212 - 2.42667 \cdot 10^{-6}\ T - 90.2725\ T^{-1} - 4.34493 \cdot 10^4\ T^{-2} + 1.59309 \cdot 10^7\ T^{-3} - 1.43688 \cdot 10^9\ T^{-4} \quad (kcal/g \cdot ℃) ,$$

where T is the absolute temperature in K, $T \geqq 3000$.

Thermal conductivity:

$$k = 0.028 \quad (cal/cm \cdot s \cdot ℃) .$$

(5) Alloy 800H[3]

Density (g/cm^3)	Specific heat (cal/g·℃)
7.95	0.12

Temperature (℃)	k (cal/cm·sec·℃)
20	0.0275
100	0.0310
200	0.0351
300	0.0389
400	0.0428
500	0.0466
600	0.0504
700	0.0545
800	0.0590
900	0.0647
1000	0.0953

(6) 2 1/4Cr-1Mo steel[4]

Temperature (℃)	Density (g/cm^3)	Specific heat (cal/g·℃)	Thermal conductivity (cal/cm·sec·℃)
20	7.81	0.107	0.0783
150	7.81	0.109	0.0780
100	7.78	0.111	0.0777
150	7.78	0.115	0.0773
200	7.75	0.119	0.0769
250	7.75	0.123	0.0766
300	7.72	0.129	0.0762
350	7.70	0.135	0.0758
400	7.70	0.141	0.0754
450	7.67	0.149	0.0751
500	7.67	0.157	0.0747
550	7.64	0.165	0.0743
600	7.61	0.172	0.0739

(7) Hastelloy XR

The thermal property of Hastelloy XR is the same as that of Hastelloy X[5]. The tabulated data of specific heat and thermal conductivity, which are listed below, are in good agreement with the experimental data of Hastelloy XR, as shown in Figs. A.2-1 and A.2-2.

Density ρ = 8.23 (g/m^3)

Specific heat C_p

Temperature (℃)	Cp (cal/g℃)
20	0.116
315	0.119
650	0.139
870	0.167
1095	0.205

Thermal conductivity k

Temperature (℃)	k (cal/cm·sec·℃)
20	0.0232
100	0.0265
200	0.0306
300	0.0351
400	0.0396
500	0.0444
600	0.0492
700	0.0544
800	0.0597
900	0.0654

(8) SUS304[4]

Temperature (℃)	Density (g/cm³)	Specific heat (cal/g℃)	Thermal conductivity (cal/cm·sec·℃)
20	8.03	0.108	0.0348
100	8.00	0.118	0.0373
200	7.95	0.125	0.0405
300	7.90	0.129	0.0437
400	7.86	0.132	0.0470
500	7.81	0.134	0.0502
600	7.76	0.138	0.0534
700	7.72	0.142	0.0567
800	7.67	0.147	0.0598

(9) Thermal insulator for low temperature service
(Calsium Silicate heat insulating material)

Temperature (℃)	Density (kg/m^3)	Specific heat (kcal/kg℃)	Thermal conductivity (kcal/mh℃)
0	200	0.20	0.046
100	200	0.21	0.056
200	200	0.22	0.066
300	200	0.23	0.076
400	200	0.24	0.086
500	200	0.25	0.096
600	200	0.26	0.106
700	200	0.27	0.116
800	200	0.28	0.126
900	200	0.29	0.136

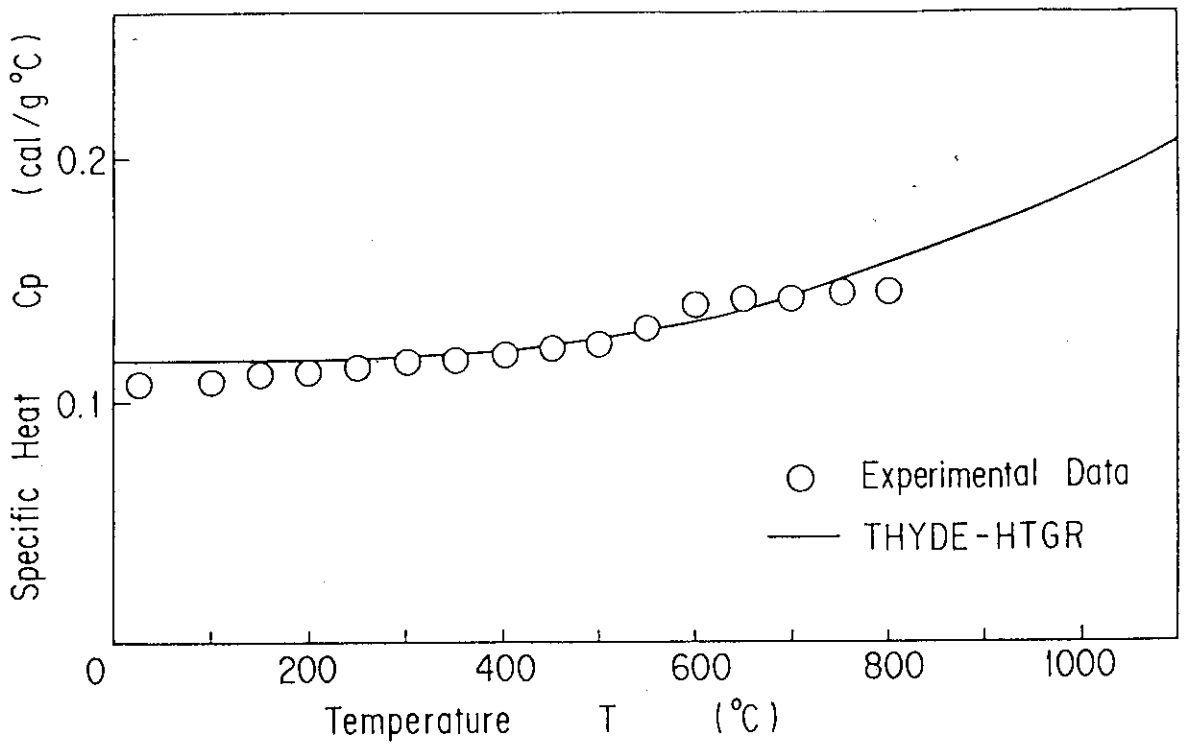

Fig. A.2-1 Specific Heat of Hastelloy XR

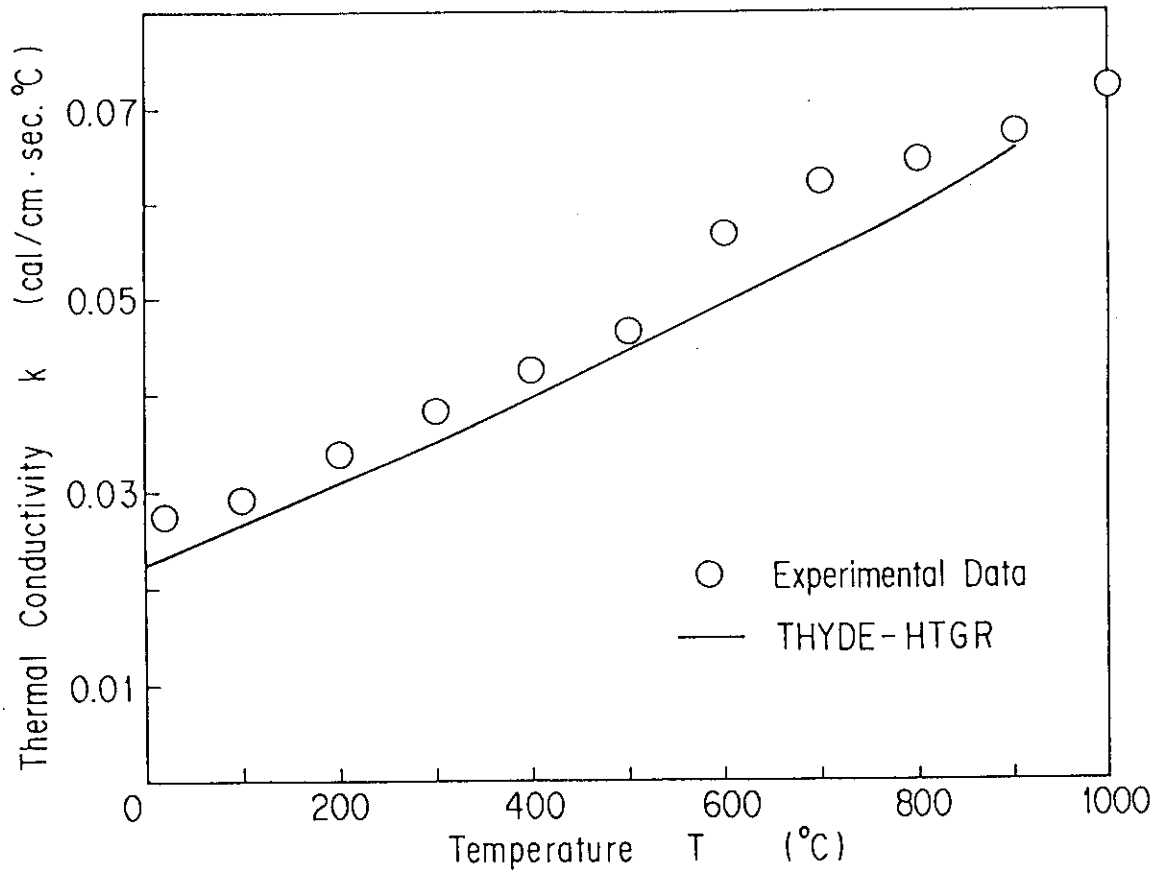

Fig. A.2-2 Thermal Conductivity of Haselloy XR

References of Appendix

1. Private communication with S. Satoh et al., (1985)

2. Safety analysis report, Use of H-451 graphite in Fort St. Vrain fuel elements, GLP-5588, General Atomic Company, (1977).
3. Private communication with Japan Iron and Steel Association, (1982).
4. YAMADA, Y. et al.: Second report of research cooperation subcomittee 46 on research and development of the methods for inelastic structural analysis, J254 79-02, June (1979).
5. NOMURA, S. et al.: Guidelines for the structural design of experimental multi-purpose VHTR at the Elevated Temperature Service, JAERI-M 6396, Jan. (1976).
6. Cederberg et al.,: Thermodynamiceskije i teplofiziceskije svojstva GELIJA, Moskau, Atomizdat, (1969).